Nondecoupling effects from heavy Higgs bosons by matching 2HDM to HEFT amplitudes

F. Arco [1,*] D. Domenech [1,†] M. J. Herrero [1,‡] and R. A. Morales [2,§]

*1Departamento de Física Teórica and Instituto de Física Teórica, IFT-UAM/CSIC,
Universidad Autónoma de Madrid, Cantoblanco, 28049 Madrid, Spain*
*2IFLP, CONICET—Departamento de Física, Universidad Nacional de La Plata,
C.C. 67, 1900 La Plata, Argentina*

In this work, we explore the low-energy effects induced from the integration of the heavy Higgs boson modes H, A, and $H^{\pm}$ within the two-Higgs-doublet model (2HDM) by assuming that the lightest Higgs boson h is the one observed experimentally at $m_h \sim 125$ GeV. We work within the context of effective field theories, focusing on the Higgs effective field theory (HEFT), although some comparisons with the Standard Model effective field theory case are also discussed through this work. Our main focus is placed in the computation of the nondecoupling effects from the heavy Higgs bosons and the capture of such effects by means of the HEFT coefficients which are expressed in terms of the input parameters of the 2HDM. Our approach to solve this issue is by matching the amplitudes of the 2HDM and the HEFT for physical processes involving the light Higgs boson h in the external legs instead of the most frequently used matching procedure at the Lagrangian level. More concretely, we perform the matching at the amplitudes level for the following physical processes, including scattering and decays: $h \to WW^* \to Wf\bar{f}'$, $h \to ZZ^* \to Zf\bar{f}$, $WW \to hh$, $ZZ \to hh$, $hh \to hh$, $h \to \gamma\gamma$, and $h \to \gamma Z$. One important point of this work is that the matching is required to happen at low energies compared to the heavy Higgs boson masses, and these are heavier than the other particle masses. The proper expansion for this heavy mass limit is also defined here, which provides the results for the nondecoupling effects presented in this work. We finally discuss the implications of the resulting effective coefficients and remark on the interesting correlations detected among them.

I. INTRODUCTION

The use of effective field theories (EFTs) to describe new physics effects from scenarios beyond the Standard Model (BSM) is nowadays a powerful and convenient tool in many aspects—first, because they are built mainly from symmetry requirements, therefore providing a model-independent framework, and, second, because the absence of new particles discoveries at the experiments indicates no preference from data for any particular fundamental underlying theory to describe the BSM physics. In the EFT context, the information on the new physics is exclusively

*francisco.arco@uam.es
†jose.domenech@estudiante.uam.es
‡maria.herrero@uam.es
§roberto.morales@fisica.unlp.edu.ar

contained in the specific values of the effective coefficients (named in different ways in the literature: Wilson coefficients, effective parameters, effective low-energy constants, etc.). On the other hand, the direct comparison with data of the predictions from EFTs for observable quantities is a valuable task and of great interest nowadays. In particular, we focus here on the EFTs that describe the BSM Higgs boson physics and that contain the Higgs boson observed experimentally with a mass value of $m_h \sim 125$ GeV [1–3]. The two most popular EFTs are the Standard Model effective field theory (SMEFT) and the Higgs effective field theory (HEFT); see, for instance, the reviews [4,5]. In contrast to the so-called κ framework, which is usually preferred by the experimental community to constraint the BSM effective couplings (also called anomalous effective couplings), these two gauge theories are well-defined quantum EFTs which are built under the gauge symmetry guiding principle. SMEFT and HEFT preserve both the gauge symmetries of the SM; i.e., they are both built from $SU(3)_C \times SU(2)_L \times U(1)_Y$ gauge-invariant effective operators and both are renormalizable theories, using the more relaxed definition of renormalization in EFTs.

This accounts for renormalization in the truncated series of effective operators for the given EFT.

In this work, we choose the HEFT to describe the BSM Higgs physics, because it is better suited for scenarios where the underlying UV theory generating such EFT at low energies could be strongly interacting. By strongly interacting dynamics, here we simply mean UV scenarios that include the possibility of large couplings, in contrast to weakly interacting scenarios where all couplings are small. We will, in particular, focus here on the bosonic part of the HEFT whose effective Lagrangian was called in its origins electroweak chiral lagrangian (EChL), in close analogy to the chiral Lagrangian (ChL) and chiral perturbation theory (ChPT) for low-energy QCD. Similarly to ChPT being the proper tool to describe the low-energy hadronic physics with QCD as the UV theory containing large couplings, the HEFT is the proper tool to describe the low-energy Higgs physics from the given UV theory containing large couplings.

Our main interest here is the use of HEFT as the proper tool to capture all the potential nondecoupling effects from the heavy BSM Higgs bosons in the case where the UV underlying theory is the well-known two-Higgs-doublet Model (2HDM); for a review, see, for instance, [6,7]. Our single assumption for the 2HDM is the following: Out of the five physical Higgs bosons, the lightest one h is identified with the observed Higgs particle, and the other four H, $H^{\pm}$, and A are assumed to be heavier than the electroweak (EW) scale, namely, heavier than $v = 246$ GeV. Given the present constraints from all experimental searches, this seems a very reasonable assumption. Then, under this assumption, the immediate question comes: What are the low-energy effects from the integration out of these heavy modes (tree and one-loop level) that could be observed in an experiment? In general, if the heavy modes leave nondecoupling effects in the low-energy observables, they could be more easily detected, in contrast to the so-called decoupling effects that leave weaker hints in the low-energy physics. To be more precise, the definition of decoupling versus nondecoupling effects in the low-energy physics is well established in the famous decoupling theorem of Appelquist and Carazzone [8]. In short, it is a statement on the behavior with the heavy particle mass of the one-particle irreducible (1PI) proper vertices with light particles in the external legs after the heavy particles have been integrated out (at any order). It says that there is decoupling when all these heavy particle effects can be absorbed into redefinitions of the couplings, parameters, and fields of the low-energy theory (i.e., renormalizing these quantities) or else they are suppressed by inverse powers of the heavy masses. In contrast, when this behavior does not happen, and the heavy particle effects in the physical observables do not decrease as inverse powers of the heavy masses (hence, leading to hints at low energies), they are said to be nondecoupling. The most clear examples of nondecoupling effects appear in theories with spontaneous

symmetry breaking and, in particular, when the particle masses are generated by a Higgs mechanism, providing a relation between the generated mass, the coupling, and the vacuum expectation value which defines the broken phase. For instance, within the SM itself, it applies to the Higgs boson case with self-coupling and mass being related by $\lambda = m_h^2/(2v^2)$. It also happens in the top quark case with Yukawa coupling and mass being related by $y_t = \sqrt{2}m_t/v$. These two particles leave nondecoupling effects (i.e., non-decreasing with inverse powers of their masses) in several observables at low energies which indeed have been explored in past experiments. For instance, in $\Delta\rho$, which defines the radiative corrections to the W and Z boson mass relation, $\rho = m_W^2/(m_Z^2 \cos^2 \theta_W)$, with respect to the tree-level prediction $\rho^{\text{tree}} = 1$. These and other nondecoupling effects from the heavy SM Higgs in the 1PI one-loop functions with external EW gauge bosons were computed long ago and collected in a set of effective coefficients of the EChL in [9,10]. Similarly, we aim to explore here the 2HDM case with the BSM heavy Higgs bosons leaving nondecoupling effects in low-energy observables which can be collected in a set of effective coefficients of the HEFT.

It should be noticed that these kind of BSM nondecoupling effects cannot be encoded within the SMEFT framework, since, by construction, the effective operators describing the BSM Higgs physics at low energies carry Wilson coefficients that are suppressed by inverse powers of the UV energy scale. Therefore, in the present case of integrating out the 2HDM heavy Higgs bosons, they lead to decoupling effects that go as inverse powers of the heavy Higgs boson masses m_{heavy}, i.e., $\sim(1/m_{\text{heavy}}^2)$ for dimension six operators, $\sim(1/m_{\text{heavy}}^4)$ for dimension eight operators, and so on. For instance, in [11], the SMEFT dimension six low-energy effects for 2HDM are derived at the Lagrangian level, and they find such decoupling behavior with the heavy mass. The necessity to move beyond dimension six interactions within the SMEFT for any scenario that contains Higgs boson mixing and the inclusion of dimension eight operator effects are discussed in [12–14], where they also find such decoupling behavior. Then, within the SMEFT, these decoupling effects from the heavy Higgs bosons disappear, in the heavy mass limit, and the 2HDM converges to the SM. The case of the HEFT is different, and the convergence of the 2HDM to the SM is reached in a different way, as will be discussed here. The relation between the HEFT and the SMEFT is by itself an interesting field of research, and it has been considered under different approaches. For instance, a geometrical approach and the issue of nondecoupling effects described by means of the HEFT, but not for the SMEFT, has also been considered in [15–20]. Some relations between the SMEFT and the HEFT, within the context of the 2HDM, have also been considered recently in [21]. They require matching at the Lagrangian level and also require decoupling and perturbativity as a principle guide, arriving to

results for the amplitudes were they find no relevant differences among HEFT and SMEFT. In summary, all effects from the 2HDM heavy Higgs bosons being described by EFTs in the previous works are found to be decoupling at low-energy observables. This is in contrast with our study here.

In this work, we will present a computation of the nondecoupling effects from the heavy Higgs bosons of the 2HDM by matching the predictions at the amplitude level of the 2HDM with the predictions from the HEFT, considering the leading effects in each observable, at either the tree level or the one-loop level depending on the process. The result of this matching will provide the values of the HEFT effective coefficients containing these nondecoupling effects. It should be noticed that, *a priori*, a nondecoupling behavior is expected to happen in the 2HDM case, because the triple Higgs couplings can have large values due to the relations of these couplings with the heavy masses. For instance, $\lambda_{hH^+H^-}$ can be large for heavy $m_{H^\pm}$, since the derived $\lambda_{hH^+H^-}$ in terms of the physical masses contains a $\mathcal{O}(m_{H^\pm}^2/v^2)$ term. One crucial difference with respect to other approaches is that we have chosen here to do this matching of predictions at the amplitude level, i.e., with observable and measurable physical quantities. In general, there are three alternatives to do matching among the UV theory and the low-energy EFT, and they are not totally equivalent. The matching can be done (i) at the Lagrangian level, (ii) at the effective action level (or, equivalently, identifying the full set of 1PI functions), and (iii) at the amplitude level. The simplest and most frequently used method in the literature is the first one. The most complete framework for matching is the second one, since it implies the identification in the two theories of all the 1PI renormalized functions with external light particles, being generically off shell. However, we have preferred to match amplitudes (with external physical particles on shell), since we believe it is more physical, free from ambiguities in field redefinitions, choice of operator basis, and renormalization prescriptions. Furthermore, it does not require the use of pseudo-observables (like in the κ framework) to connect with data, since the prediction of the amplitude is directly comparable with data. By requiring the matching at the amplitude level between the predictions from the HEFT and the 2HDM with large heavy Higgs masses and solving these matching equations, we will be able to extract the values of the HEFT coefficients in terms of the 2HDM input parameters. These are chosen here to be the physical masses m_h, m_H, $m_{H^\pm}$, and m_A, the ratio of the two Higgs vacuum expectation values (vevs), $\tan\beta$, the parameter $\cos(\beta - \alpha)$, and the Z_2 soft-breaking mass parameter m_{12}. To be more precise, we do the matching of the 2HDM and HEFT amplitudes after performing a large mass expansion of the 2HDM amplitude in terms of the inverse powers of the heavy Higgs boson masses. Notice that this is a

well-defined and convergent expansion, as will be shown here. We have selected to match the amplitudes of some specific processes (scattering and decays) involving the light Higgs boson in the external legs which contain the most relevant nondecoupling effects. Concretely, $h \to WW^* \to Wf\bar{f}'$, $h \to ZZ^* \to Zf\bar{f}$, $WW \to hh$, $ZZ \to hh$, $hh \to hh$, $h \to \gamma\gamma$, and $h \to \gamma Z$. The explicit computations of the 2HDM amplitudes for these processes will be presented and discussed here. Some of these processes have also been considered within the HEFT previously in the literature for different purposes. In particular, $WW \to hh$, $h \to \gamma\gamma$, and $h \to \gamma Z$ have been computed within the next-to-leading-order (NLO) HEFT including renormalization of the one-loop corrections and doing the computation in a generic R_ξ gauge [22–24]. The cases of $WW \to hh$ and $hh \to hh$ scattering processes have also been studied within the NLO HEFT in [5,25–28]. The Higgs decays $h \to WW^* \to Wf\bar{f}'$, $h \to ZZ^* \to Zf\bar{f}$, $h \to \gamma\gamma$, and $h \to \gamma Z$ and the vector boson fusion scattering $VV \to hh$ have also been studied within the NLO HEFT in [29] focusing in the implications for LHC physics. In the present paper, it will be shown that, in order to capture the leading nondecoupling effects from the 2HDM heavy Higgs bosons in these processes, it is sufficient to do the matching at $\mathcal{O}(\hbar^0)$ in all cases except in the $h \to \gamma\gamma$ and $h \to \gamma Z$ decays, where the matching must be done at $\mathcal{O}(\hbar^1)$. Once we solve analytically these matching equations and find the expressions of the effective coefficients in terms of the 2HDM input parameters, we will analyze the predictions for those coefficients, both analytically and numerically. We will do that analysis in several interesting scenarios that, following the usual terminology, we classify as (i) alignment $[\cos(\beta - \alpha) = 0]$, (ii) misalignment $[\cos(\beta - \alpha) \neq 0]$, and (iii) quasialignment $[\cos(\beta - \alpha) \ll 1]$. In the final part of this work, we will discuss on the interesting correlations found here among the HEFT coefficients in these three different limits.

The paper is organized as follows: Section II provides a brief introduction to the HEFT focusing on its comparison to the SMEFT approach. The relevant part of the HEFT Lagrangian for the present computation is also included in this section. Section III contains the relevant details of the 2HDM, in particular, the expressions of the derived triple Higgs couplings in terms of the selected input parameters of this model. The analytical expressions of the amplitudes for the considered processes in the SM, HEFT, and 2HDM are collected in Sec. IV. The matching procedure is described in Sec. V. The way to the solution for the HEFT coefficients in terms of the input 2HDM parameters that summarizes the nondecoupling effects in the heavy mass limit is also included in this section. Also, the correlations found among the HEFT coefficients from the 2HDM are presented in this section. The numerical analysis of the previous results are presented in Sec. VI. Finally, we conclude in Sec. VII. The details of the

Feynman rules and the one-loop functions are given in the Appendixes.

II. HEFT VERSUS SMEFT

As stated above, we have focused in this paper on the HEFT. However, before reviewing the details of the HEFT Lagrangian that are needed for the present computation, we would like first to comment shortly on the most relevant aspects that crucially differentiate HEFT versus SMEFT. These differences will allow us to better understand the decoupling versus the nondecoupling effects of the heavy Higgs boson modes in the two low-energy theories.

The main differences between these two EFTs can be summarized as follows. (i) In the SMEFT the Higgs boson is introduced as a component of a $SU(2)$ doublet, whereas in the HEFT it is introduced as a singlet. (ii) The would-be Goldstone bosons (GBs) associated to the EW symmetry breaking, $SU(2)_L \times U(1)_Y \to U(1)_{em}$, in the SMEFT are identified with the other components in this doublet, therefore completing together the simplest linear realization. In contrast, in the HEFT, the GBs transform nonlinearly under the global symmetry of the scalar sector $SU(2)_L \times SU(2)_R$, usually called the EW chiral symmetry, and they are frequently parametrized by an exponential function. (iii) The ordering of the effective operators in the SMEFT is done in terms of the canonical dimension (cd = 4, 6, 8, etc.), whereas in the HEFT this ordering is done in terms of the chiral dimension (chd = 2, 4, etc.). This different counting (cd versus chd) leads to a different classification in both theories of what is the leading order (LO) versus what is the NLO. The ordering in cd implies that the LO SMEFT Lagrangian with cd = 4 is the SM Lagrangian, the NLO SMEFT includes the cd = 6 operators with coefficients being suppressed by inverse powers of the ultraviolet (UV) Λ scale, as $\sim \Lambda^{-2}$, and so on. In contrast, the HEFT reaches the SM for an specific choice of the effective coefficients in the LO Lagrangian with chd = 2 and setting the NLO effective coefficients to zero. (iv) The predictions for observables in both EFTs are also very different. In particular, the HEFT, due to the chd counting (involving derivatives and soft masses), provides predictions for the amplitudes of physical processes that are organized typically as expansions in powers of the relevant process energy (and powers of the soft masses involved). This is not the case in the SMEFT, which, in contrast, provides predictions for the amplitudes that are organized in terms of the expansion in inverse powers of Λ. (v) The renormalization programs in both EFTs are also very different. In the SMEFT, all the operators are renormalized together, without doing any distinction in the renormalization procedure between the LO and the NLO contributions. In contrast, in the HEFT, there is a hierarchy in the renormalization procedure between the LO and the NLO contributions. In the chiral counting the divergent loops

computed with the LO Lagrangian (chd = 2) are renormalized by the effective coefficients of the NLO Lagrangian (chd = 4), providing a well-defined framework for renormalization to one-loop order (like in ChPT), with a marked hierarchy LO/NLO and where the relevant scale in this loop counting is given typically by $4\pi v \sim 3$ TeV. The one-loop renormalization program in the bosonic sector of the HEFT has been studied using a R_ξ general covariant gauge in [22–24]. The renormalization in the SMEFT, via the renormalization group equations, was studied in [30–32]. The SMEFT for R_ξ gauges was studied in [33,34]. Some illustrative discussion on the matching at the 1PI functions level can also be found in [35]. On the other hand, the matching of tree-level amplitudes predicted by the HEFT and the SMEFT also leads to some relations between the HEFT and the SMEFT coefficients [36]. But all these attempts of matchings among the HEFT and the SMEFT provide just partial relations among these two theories, since they assume a specific given order in the expansion of both theories (LO, NLO, etc.) and also a given order in the loop expansion [i.e., in the $\mathcal{O}(\hbar^n)$ expansion], so they are not complete comparisons. Furthermore, to conclude that one theory contains the other one should proceed with a complete comparison of the full quantum EFTs (i.e., not truncated, and to all orders in the loop expansion). But this is a difficult task.

Next, we proceed with the short summary of the needed ingredients of the HEFT Lagrangian for the present computation. For this presentation and the notation, we follow closely [22–24]. First, we recall that in the bosonic sector the active degrees of freedom are the EW gauge bosons B_μ and W_μ^a ($a = 1, 2, 3$), their corresponding GBs π^a ($a = 1, 2, 3$), and the Higgs boson h. The Lagrangian is invariant under EW gauge, $SU(2)_L \times U(1)_Y$, transformations, and the scalar sector of the EChL has an additional invariance under the EW chiral $SU(2)_L \times SU(2)_R$ symmetry. The Higgs boson field is invariant under all transformations; i.e., it is a singlet of the EW chiral symmetry and the EW gauge symmetry. Therefore, the interactions of h are introduced via generic polynomials, since there are not limitations from symmetry arguments. On the other hand, the GBs π^a ($a = 1, 2, 3$) transform nonlinearly under this EW chiral transformation. Then they are introduced in a nonlinear representation via the exponential parametrization, by means of the matrix U, which transforms linearly under the EW chiral transformations:

$$U(\pi^a) = e^{i\pi^a \tau^a / v}, \qquad (2.1)$$

where τ^a, $a = 1, 2, 3$, are the Pauli matrices and $v = 246$ GeV. In addition, the EW gauge bosons are introduced by the gauge invariance principle, and they appear in the following combinations:

$$\hat{B}_\mu = g' B_\mu \tau^3/2, \qquad \hat{W}_\mu = g W_\mu^a \tau^a/2,$$

$$D_\mu U = \partial_\mu U + i\hat{W}_\mu U - iU\hat{B}_\mu, \qquad \hat{B}_{\mu\nu} = \partial_\mu \hat{B}_\nu - \partial_\nu \hat{B}_\mu,$$

$$\hat{W}_{\mu\nu} = \partial_\mu \hat{W}_\nu - \partial_\nu \hat{W}_\mu + i[\hat{W}_\mu, \hat{W}_\nu]. \tag{2.2}$$

In the chiral dimension counting, all derivatives and masses count as momentum:

$$\partial_\mu, \quad m_W, \quad m_Z, \quad m_h, \quad gv, \quad g'v, \quad \lambda v \sim \mathcal{O}(p). \tag{2.3}$$

The HEFT organizes the effective operators in the EChL into terms with increasing chiral dimension, starting at chd $= 2$, then chd $= 4$, and so on. Notice again that this chiral counting differs from the usual SMEFT expansion with operators having growing canonical dimension, starting at cd $= 4$, then cd $= 6$. etc., and terms suppressed with the heavy scale Λ.

For the bosonic sector of the HEFT, we consider the leading-order Lagrangian, with chiral dimension two, $\mathcal{L}_2$, and the next-to-leading-order one with chiral dimension four, $\mathcal{L}_4$:

$$\mathcal{L}_{\text{HEFT}} = \mathcal{L}_{\text{EChL}} = \mathcal{L}_2 + \mathcal{L}_4. \tag{2.4}$$

First, the leading-order Lagrangian is given by

$$\mathcal{L}_2 = \frac{v^2}{4}\left(1 + 2a\frac{h}{v} + b\left(\frac{h}{v}\right)^2 + \cdots\right)\text{Tr}[D_\mu U^\dagger D^\mu U]$$

$$+ \frac{1}{2}\partial_\mu h \partial^\mu h - V_{\text{EChL}}(h) - \frac{1}{2g^2}\text{Tr}[\hat{W}_{\mu\nu}\hat{W}^{\mu\nu}]$$

$$- \frac{1}{2g'^2}\text{Tr}[\hat{B}_{\mu\nu}\hat{B}^{\mu\nu}] + \mathcal{L}_{\text{GF}} + \mathcal{L}_{\text{FP}}. \tag{2.5}$$

Here, $V_{\text{EChL}}(h)$ is the EChL Higgs potential, and $\mathcal{L}_{\text{GF}}$ and $\mathcal{L}_{\text{FP}}$ are the gauge-fixing and Faddeev-Popov Lagrangian, respectively. The dots stand for terms that do not enter in our processes of interest, neither at tree level nor at one-loop level. The EChL Higgs potential in $\mathcal{L}_2$ is given by

$$V_{\text{EChL}}(h) = \frac{m_h^2}{2}h^2 + \kappa_3 \lambda v h^3 + \kappa_4 \frac{\lambda}{4}h^4, \tag{2.6}$$

where $m_h^2 = 2\lambda v^2$ as in the SM and values for κ_3 and κ_4 different from 1 encode the physics beyond SM.

We implement the linear covariant R_ξ gauges [37] with the gauge-fixing Lagrangian, given by

$$\mathcal{L}_{\text{GF}} = -F_+F_- - \frac{1}{2}F_Z^2 - \frac{1}{2}F_A^2$$

$$= -\frac{1}{\xi}(\partial^\mu W_\mu^+ - \xi m_W \pi^+)(\partial^\mu W_\mu^- - \xi m_W \pi^-)$$

$$- \frac{1}{2\xi}(\partial^\mu Z_\mu - \xi m_Z \pi^3)^2 - \frac{1}{2\xi}(\partial^\mu A_\mu)^2, \tag{2.7}$$

and the corresponding Faddeev-Popov Lagrangian [38], given by

$$\mathcal{L}_{\text{FP}} = \sum_{i,j=+,-,Z,A} \bar{c}^i \frac{\delta F_i}{\delta \alpha_j} c^j, \tag{2.8}$$

where ξ is the generic gauge-fixing parameter of the R_ξ gauges, c^j are the ghost fields, and α_j ($j = +, -, Z, A$) are the corresponding gauge transformation parameters. Notice that $\mathcal{L}_{\text{GF}}$ in Eq. (2.7) is the same as in the SM and for the 2HDM. Formally, the expressions in Eq. (2.8) are also the same as in the SM and 2HDM. However, the Higgs and GBs transformations in this nonlinear EFT differ from the corresponding ones in the SM, yielding to different interactions among those scalars and the ghost fields.

In the case that a given observable require a one-loop computation with the $\mathcal{L}_2$ terms, the $\mathcal{L}_4$ operators must be included in order to be consistent with the chiral counting and also to use the coefficients in $\mathcal{L}_4$ as counterterms to renormalize the divergences generated by the loops from $\mathcal{L}_2$, following the usual procedure with chiral Lagrangians. For the present work, we will compute the one-loop Higgs decays $h \to \gamma\gamma$ and $h \to \gamma Z$; then the relevant terms of the next-to-leading-order contributions are included in the following Lagrangian [22–24]:

$$\mathcal{L}_4 = -\left(a_{HBB}\frac{h}{v} + a_{HHBB}\frac{h^2}{v^2}\right)\text{Tr}[\hat{B}_{\mu\nu}\hat{B}^{\mu\nu}]$$

$$- \left(a_{HWW}\frac{h}{v} + a_{HHWW}\frac{h^2}{v^2}\right)\text{Tr}[\hat{W}_{\mu\nu}\hat{W}^{\mu\nu}]$$

$$+ \left(a_{H1}\frac{h}{v} + a_{HH1}\frac{h^2}{v^2}\right)\text{Tr}[U\hat{B}_{\mu\nu}U^\dagger\hat{W}^{\mu\nu}] + \cdots, \tag{2.9}$$

where the relevant coefficients for the Higgs decays under consideration, $h \to \gamma\gamma$ and $h \to \gamma Z$, are given in terms of the coefficients in Eq. (2.9) by the following relations:

$$a_{h\gamma\gamma} = a_{HBB} + a_{HWW} - a_{H1}, \tag{2.10}$$

$$a_{h\gamma Z} = \frac{1}{c_w^2}\left(-a_{HBB}s_w^2 + a_{HWW}c_w^2 - \frac{1}{2}a_{H1}(c_w^2 - s_w^2)\right). \tag{2.11}$$

These coefficients in Eq. (2.9) and others (see Refs. [22–24]) also enter in other observables when they are predicted at the one-loop level. In addition to the mentioned scattering amplitudes $WW \to hh$ and $ZZ \to hh$, these coefficients will also enter in other vector boson scattering amplitudes for double Higgs production when computed to one loop like $\gamma\gamma \to hh$ and $\gamma Z \to hh$. Nevertheless, we do not study these one-loop amplitudes here, since the focus of our interest is to capture the most relevant nondecoupling effects from the heavy modes of the UV theory, which,

as we will see, are summarized in the tree-level coefficients from $\mathcal{L}_2$, a, b, κ_3, and κ_4 and in the NLO coefficients from $\mathcal{L}_4$, $a_{h\gamma\gamma}$, and $a_{h\gamma Z}$.

One important point to recall is the way the SM is embedded within the HEFT. It is clear that the comparison cannot be done at the Lagrangian level, since within the SM the Higgs field is introduced into a doublet, whereas in the HEFT it is a singlet. Thus, the Lagrangians themselves are not directly comparable. The Feynman rules for the couplings with scalar fields (h and the GBs) are also different in the HEFT and the SM due to the nonlinear parametrization used in the HEFT. Thus, the comparison between the SM and the HEFT should be done via their predictions for the observables instead of via their corresponding Lagrangians. Specifically, in order to reach the SM predictions from the HEFT predictions, one has to fix the HEFT coefficients as follows: (i) The LO coefficients must be set to the following particular values: $a = 1$, $b = 1$, $\kappa_3 = 1$, and $\kappa_4 = 1$. Equivalently, if we write the coefficients in terms of the corresponding Δ's, which are defined by $a = 1 - \Delta a$, $b = 1 - \Delta b$, $\kappa_3 = 1 - \Delta\kappa_3$, and $\kappa_4 = 1 - \Delta\kappa_4$, then the SM predictions can be obtained from the HEFT predictions by setting $\Delta a = 0$, $\Delta b = 0$, $\Delta\kappa_3 = 0$, and $\Delta\kappa_4 = 0$. Additionally, all the NLO coefficients must also be set to zero; i.e., generically, $a_i = 0$ for all coefficients in $\mathcal{L}_4$.

We have summarized the Feynman rules of the HEFT that are relevant for the present computation in Table I in Appendix A (for a full set see Refs. [22–24]). The corresponding Feynman rules of the SM are also included for comparison.

The embedding of the SM into the SMEFT is very different than in the HEFT, since the SM Lagrangian is explicitly included in the SMEFT Lagrangian as its first term contribution of canonical dimension 4:

$$\mathcal{L}_{\text{SMEFT}} = \mathcal{L}_{\text{SM}} + \mathcal{L}_6 + \mathcal{L}_8 + \cdots, \quad \text{with} \quad \mathcal{L}_d = \frac{c_i}{\Lambda^{d-4}} \mathcal{O}_i^{(d)}.$$
(2.12)

And both the SM and the SMEFT place the Higgs boson into the standard Higgs doublet. It is usually parametrized as follows:

$$\Phi = \begin{pmatrix} -i\pi^+ \\ \frac{v+h-i\pi^3}{\sqrt{2}} \end{pmatrix} = \begin{pmatrix} G^+ \\ \frac{v+h+iG^0}{\sqrt{2}} \end{pmatrix}.$$
(2.13)

Thus, to reach the SM predictions from the SMEFT predictions, this can be done at the Lagrangian level, by simply setting all Wilson coefficients c_i to zero in the Lagrangian terms with canonical dimension 6, 8, etc.

Finally, before ending this section, it is worth recalling the previous relations found in [36] among the HEFT and SMEFT coefficients by the same procedure that we choose in the present paper of matching amplitudes. This matching

was done for the particular scattering process $WW \to hh$, and the assumption for both EFTs was to work at the tree level and with the truncated Lagrangian $\mathcal{L}_2 + \mathcal{L}_4$ for the HEFT and the truncated Lagrangian up to cd = 8 for the SMEFT. The result of this matching provides interesting relations among the effective coefficients of both theories. These include the following relations (for a full set see Ref. [36]):

$$\Delta a|_{\text{SMEFT}} = -\frac{1}{4}\frac{v^2}{\Lambda^2}\delta c_{\phi D},$$

$$\Delta b|_{\text{SMEFT}} = -\frac{v^2}{\Lambda^2}\delta c_{\phi D},$$

$$\Delta\kappa_3|_{\text{SMEFT}} = -\frac{5}{4}\frac{v^2}{\Lambda^2}\delta c_{\phi D},$$

$$a_{HWW}|_{\text{SMEFT}} = -\frac{v^2}{2m_W^2}\frac{v^2}{\Lambda^2}c_{\phi W},$$

$$a_{HHWW}|_{\text{SMEFT}} = -\frac{v^2}{4m_W^2}\frac{v^2}{\Lambda^2}c_{\phi W}, \qquad (2.14)$$

where the definitions for the Wilson coefficients c_i above can also be found in the mentioned reference (there, a different notation a_i was used instead of the c_i here). It is interesting to note that the above relations among the coefficients of the HEFT and the SMEFT occur across the different orders in both EFTs. In particular, LO coefficients of chd = 2 in the HEFT appear related to coefficients of cd = 6 in the SMEFT, NLO coefficients of chd = 4 in the HEFT are related to coefficients of cd = 6 in the SMEFT (and also to the coefficients of cd = 8), and so on. This also implies that capturing the nondecoupling effects using the HEFT, i.e., effects nonsuppressed by inverse powers of the heavy mass of the UV underlying theory, cannot be reproduced by the SMEFT, since by construction all the UV effects in the SMEFT are suppressed by inverse powers of the heavy scale; i.e., they produce contributions in the amplitudes of $\mathcal{O}(1/\Lambda^2)$, $\mathcal{O}(1/\Lambda^4)$, etc., and they all decouple for large Λ. Finally, it is worth mentioning that the previous values in Eq. (2.14) also indicate the existence of correlations among HEFT coefficients when they are matched to the SMEFT. In particular, in the subset given above, they are correlated as $\Delta b|_{\text{SMEFT}} = 4\Delta a|_{\text{SMEFT}}$ and $a_{HWW}|_{\text{SMEFT}} = 2a_{HHWW}|_{\text{SMEFT}}$.

III. HEAVY HIGGS BOSONS WITHIN THE 2HDM

In this section, we recall the basic aspects of the 2HDM that are relevant for the present computation. The 2HDM is the simplest extension of the SM that includes two Higgs doublets, Φ_1 and Φ_2, instead of one doublet Φ. These two doublets are linear parametrizations of the four complex scalar fields (hence, eight real scalar fields) defining the 2HDM scalar sector. They are usually defined as

$$\Phi_1 = \begin{pmatrix} \phi_1^+ \\ \frac{1}{\sqrt{2}}(v_1 + \rho_1 + i\eta_1) \end{pmatrix}, \quad \Phi_2 = \begin{pmatrix} \phi_2^+ \\ \frac{1}{\sqrt{2}}(v_2 + \rho_2 + i\eta_2) \end{pmatrix},$$

(3.1)

where v_1 and v_2 are the real VEVs acquired by the fields Φ_1 and Φ_2, respectively, with $\tan\beta = v_2/v_1$, and they satisfy the relation $v = \sqrt{(v_1^2 + v_2^2)}$, where $v = 246$ GeV is the SM VEV. The eight degrees of freedom above, $\phi_{1,2}^\pm$, $\rho_{1,2}$, and $\eta_{1,2}$, give rise to three Goldstone bosons $G^\pm$ and G^0 and five massive physical scalar fields: two CP-even scalar fields h and H, one CP-odd one A, and one charged pair $H^\pm$. Here, the mixing angles α and β diagonalize the CP-even and -odd sectors, respectively. These rotations define the physical mass eigenstates h, H, A, and $H^\pm$ in terms of the EW interaction eigenstates (or the other way around) and are given by

$$\phi_1^\pm = \cos\beta\, G^\pm - \sin\beta\, H^\pm,$$
$$\phi_2^\pm = \sin\beta\, G^\pm + \cos\beta\, H^\pm,$$
$$\eta_1 = \cos\beta\, G^0 - \sin\beta\, A,$$
$$\eta_2 = \sin\beta\, G^0 + \cos\beta\, A,$$
$$\rho_1 = \cos\alpha\, H - \sin\alpha\, h,$$
$$\rho_2 = \sin\alpha\, H + \cos\alpha\, h.$$

The relations among the two usual notations for the GBs inside the doublets are as in Eq. (2.13), i.e., $G^\pm = -i\pi^\pm$ and $G^0 = -\pi^0$.

The self-interactions among the above scalar fields are provided by the 2HDM potential. Since a general potential with two Higgs doublets can lead to flavor-changing neutral currents at the tree level, which are strongly discouraged by experimental measurements, we will impose a Z_2 symmetry [39,40] meaning invariance under $\Phi_1 \to \Phi_1$ and $\Phi_2 \to -\Phi_2$. Furthermore, we will allow this Z_2 symmetry to be only softly broken by the parameter m_{12}^2, which has dimensions of mass squared. Thus, the relevant potential for the present work of the CP-conserving 2HDM with the Z_2 soft breaking included, expressed in terms of the two doublets Φ_1 and Φ_2, is given by [6,7,39]

$$V_{2\mathrm{HDM}}(\Phi_1, \Phi_2) = m_{11}^2(\Phi_1^\dagger \Phi_1) + m_{22}^2(\Phi_2^\dagger \Phi_2) - m_{12}^2(\Phi_1^\dagger \Phi_2$$
$$+ \Phi_2^\dagger \Phi_1) + \frac{\lambda_1}{2}(\Phi_1^\dagger \Phi_1)^2 + \frac{\lambda_2}{2}(\Phi_2^\dagger \Phi_2)^2$$
$$+ \lambda_3(\Phi_1^\dagger \Phi_1)(\Phi_2^\dagger \Phi_2) + \lambda_4(\Phi_1^\dagger \Phi_2)(\Phi_2^\dagger \Phi_1)$$
$$+ \frac{\lambda_5}{2}[(\Phi_1^\dagger \Phi_2)^2 + (\Phi_2^\dagger \Phi_1)^2].$$

(3.2)

After the EW symmetry breaking, $SU(2)_L \times U(1)_Y \to U(1)_{\mathrm{em}}$, the minimization conditions for the above 2HDM potential lead to the existence of five physical

Higgs bosons: two CP-even Higgs bosons h and H, one CP-odd Higgs boson A, and two charged Higgs bosons $H^\pm$ with masses given by m_h, m_H (with $m_h < m_H$), m_A, and $m_{H^\pm}$, respectively. In addition, the three would-be Goldstone bosons disappear from the physical spectrum and provide the needed physical masses for the EW gauge bosons m_W and m_Z. In this work, we will identify the h state with the Higgs boson discovered in the LHC with a mass $m_h = 125$ GeV [1–3]. The other Higgs bosons will be assumed here to be heavier than the EW scale v, a hypothesis which is well justified given the present tight experimental constraints [41,42].

The previous potential also contains the self-interactions among the scalars of the 2HDM which are very relevant for the present work. In addition, the interactions of the Higgs bosons with the gauge bosons are given by the gauge-invariant Lagrangian built with the covariant derivatives of the two doublets and the interactions with fermions are given by the Yukawa part of the 2HDM Lagrangian. They are well known in the literature, and we do not explicit them here for shortness (see, for instance, [6,7,39]). The set of Feynman rules within the 2HDM that are relevant for the present computation are summarized in Table I in Appendix A.

In order to make predictions for observables, one may use different choices for the 2HDM input parameters. Here, since we are going to consider later the hypothesis of very heavy BSM Higgs bosons and to deal with the expansion at large heavy masses, we believe that the most convenient choice for the input parameters should contain the physical Higgs masses. Concretely, we choose in this work the following 2HDM input parameters:

$$v, \quad m_h, \quad m_H, \quad m_A, \quad m_{H^\pm}, \quad t_\beta, \quad c_{\beta-\alpha}, \quad m_{12}, \quad (3.3)$$

where we have adopted the shorthand notation $\cos x = c_x$, $\sin x = s_x$, and $\tan x = t_x$. All the remaining 2HDM parameters and couplings are, therefore, derived quantities.

The choice of $c_{\beta-\alpha}$ as an input parameter is motivated by the so-called *alignment limit*, defined as $c_{\beta-\alpha} = 0$. Under this limit, the interactions of h with the gauge bosons and with the fermions recover their SM values. For example, the h (H) coupling to WW and ZZ relative to the SM is given by $s_{\beta-\alpha}$ ($c_{\beta-\alpha}$). Currently, the measurements of the Higgs boson signal strengths are compatible with the SM prediction (within the experimental uncertainties), and, therefore, the parameter $c_{\beta-\alpha}$ is constrained to be not far away from the alignment limit (see, for instance, [41,42]). This motivates our posterior study being classified into three qualitative different scenarios defined as (i) alignment, defined by setting $c_{\beta-\alpha} = 0$, (ii) misalignment, defined by arbitrary $c_{\beta-\alpha} \neq 0$, and (iii) quasialignment, defined by $c_{\beta-\alpha} \ll 1$. As we will see in Sec. V, the solutions for the matching will differ in these three situations.

It is convenient to have in mind that taking the alignment condition does not imply the absence of BSM interactions,

because several couplings, in addition to the SM ones, remain nonvanishing when $c_{\beta-\alpha} = 0$, indeed, some of them involving the light Higgs boson h. For example, the couplings hHH, hAA, hH^+H^-, ZHA, γH^+H^-, $hhHH$, $hhAA$, hhH^+H^-, and others do not vanish in the alignment limit. This implies that the integration out of the heavy modes H, A, and $H^\pm$ could leave some nondecoupling effects that differentiate the 2HDM with respect to the SM via these couplings that could leave an important track at low-energy observables, at both tree and one-loop levels. This is our main motivation in this work and will be discussed in the following sections.

One interesting phenomenological feature of the 2HDM compared to the SM is the existence of triple and quartic interactions between the new scalar states. The 2HDM prediction of these couplings can be written in terms of the input parameters in Eq. (3.3). Under our notation, the tree-level Feynman rules of the scalar interactions involving the light Higgs that are relevant to this work are given in Table I in Appendix A and are summarized also here:

$$i\Gamma_{hhh} = -6iv\lambda_{hhh}, \tag{3.4}$$

$$i\Gamma_{hhH} = -2iv\lambda_{hhH}, \tag{3.5}$$

$$i\Gamma_{hH^+H^-} = -iv\lambda_{hH^+H^-}, \tag{3.6}$$

$$i\Gamma_{hhhh} = -6i\lambda_{hhhh}, \tag{3.7}$$

where we are following the notation from [41,42]. Other scalar interactions involving the light Higgs like Γ_{hHH}, Γ_{hHH}, and Γ_{hAA} do not participate in the present computation and are not given explicitly here, for shortness. One important aspect in this work is that these triple and quartic couplings above are not input parameters, but instead they are derived parameters. Thus, once the input parameters have been fixed to those in Eq. (3.3), the derived couplings for the physical eigenstates, i.e., the λ_x couplings, are fixed in terms of the input parameters at a given order in the loop expansion. In particular, at the tree level, these derived λ_x couplings are given by

$$v^2\lambda_{hhh} = s_{\beta-\alpha}(1 + 2c_{\beta-\alpha}^2)\frac{m_h^2}{2} - s_{\beta-\alpha}c_{\beta-\alpha}^2\frac{m_{12}^2}{s_\beta c_\beta} + c_{\beta-\alpha}^3\cot 2\beta\left(m_h^2 - \frac{m_{12}^2}{s_\beta c_\beta}\right), \tag{3.8}$$

$$v^2\lambda_{hhH} = \frac{c_{\beta-\alpha}}{2}\left(-2(3c_{\beta-\alpha}^2 - 2)\frac{m_{12}^2}{s_\beta c_\beta} - 2c_{\beta-\alpha}s_{\beta-\alpha}\cot 2\beta\left(-3\frac{m_{12}^2}{s_\beta c_\beta} + 2m_h^2 + m_H^2\right) + (2c_{\beta-\alpha}^2 - 1)(2m_h^2 + m_H^2)\right), \tag{3.9}$$

$$v^2\lambda_{hH^+H^-} = \left(m_h^2 + 2m_{H^\pm}^2 - 2\frac{m_{12}^2}{s_\beta c_\beta}\right)s_{\beta-\alpha} + 2\cot 2\beta\left(m_h^2 - \frac{m_{12}^2}{s_\beta c_\beta}\right)c_{\beta-\alpha}, \tag{3.10}$$

$$v^2\lambda_{hhhh} = \frac{m_h^2}{2} + \frac{c_{\beta-\alpha}^2}{2}\left(-4s_{\beta-\alpha}^2\frac{m_{12}^2}{s_\beta c_\beta} + 4c_{\beta-\alpha}^2\cot^2 2\beta\left(-\frac{m_{12}^2}{s_\beta c_\beta} + c_{\beta-\alpha}^2 m_h^2 + s_{\beta-\alpha}^2 m_H^2\right)\right.$$
$$+ 4c_{\beta-\alpha}s_{\beta-\alpha}\cot 2\beta\left(-2\frac{m_{12}^2}{s_\beta c_\beta} + (2c_{\beta-\alpha}^2 + 1)m_h^2 + (1 - 2c_{\beta-\alpha}^2)m_H^2\right)$$
$$\left. + 4c_{\beta-\alpha}^4(m_H^2 - m_h^2) - 4c_{\beta-\alpha}^2 m_H^2 + 3m_h^2 + m_H^2\right), \tag{3.11}$$

where, to present more compact formulas, we have included some derived parameters in these formulas like $s_{\beta-\alpha}$, s_β, c_β, and $\cot 2\beta$, that are related with the input parameters $c_{\beta-\alpha}$ and $\tan \beta$ by the following trigonometric identities:

$$s_{\beta-\alpha} = \sqrt{1 - c_{\beta-\alpha}^2}, \qquad s_\beta = \frac{t_\beta}{\sqrt{1 + t_\beta^2}}, \qquad c_\beta = \frac{1}{\sqrt{1 + t_\beta^2}}, \qquad \cot 2\beta = \frac{1 - t_\beta^2}{2t_\beta}. \tag{3.12}$$

For the discussion in the following sections, it is interesting to display the specific values of the couplings above in the simplest scenario with alignment, i.e., for $c_{\beta-\alpha} = 0$, which are named λ_x^{al} here:

$$v^2 \lambda^{\text{al}}_{hhh} = \frac{m_h^2}{2},$$

$$v^2 \lambda^{\text{al}}_{hhH} = 0,$$

$$v^2 \lambda^{\text{al}}_{hH^+H^-} = m_h^2 + 2m_{H^\pm}^2 - 2\frac{m_{12}^2}{s_\beta c_\beta},$$

$$v^2 \lambda^{\text{al}}_{hhhh} = \frac{m_h^2}{2}. \qquad (3.13)$$

We see that, in the alignment limit, λ_{hhh} and λ_{hhhh} tend to $\lambda = m_h^2/(2v^2)$, which give, respectively, the triple and quartic Higgs couplings predicted by the SM. The triple coupling of the two light Higgs bosons to one heavy Higgs boson vanishes in the alignment limit. However, the coupling of one light Higgs boson to two charged Higgs bosons is not vanishing. Regarding the above value of $\lambda^{\text{al}}_{hH^+H^-}$, we confirm that the size of this triple coupling can be very large for large input values of $m_{H^\pm}$. For instance, values of $m_{H^\pm} \sim 800$ GeV can provide large couplings of $\lambda^{\text{al}}_{hH^+H^-} \sim \mathcal{O}(10)$ which, according to the detailed analysis in [41,42], are yet allowed by all the present theoretical and experimental constraints. This is the situation in which we are interested in this work. Then, when doing a large mass expansion of the amplitudes in the following sections, we simply mean an expansion in powers of a small dimensionless parameter $\sim (v/m_{\text{heavy}})$ which should be convergent whenever $v/m_{\text{heavy}} \ll 1$. Thus, we have in mind that our forthcoming results for heavy boson masses m_H, m_A, and $m_{H^\pm}$, which are collectively named m_{heavy}, should apply for these masses being above v and close to the TeV scale.

Within the 2HDM, the Higgs couplings to fermions also differ with respect to the SM. However, since in this work we consider only interactions in the bosonic sector of the 2HDM, they are not relevant to this work, and we will not describe them here.

IV. ANALYTICAL RESULTS OF THE AMPLITUDES

In this section, we present the amplitudes for the different observables considered in this work. We focus on the following scattering and decay processes that involve the light Higgs boson and EW gauge bosons in the external legs: $h \to WW^* \to Wf\bar{f}'$, $h \to ZZ^* \to Zf\bar{f}$, $W^+W^- \to hh$, $ZZ \to hh$, $hh \to hh$, $h \to \gamma\gamma$, and $h \to \gamma Z$. All these amplitudes were computed for the three models under consideration, SM, HEFT, and 2HDM, using an arbitrary R_ξ gauge and verifying the gauge parameter ξ independence for the on-shell amplitudes. Thus, all the results presented here for the amplitudes are gauge invariant, as expected.

The following expressions were obtained using FeynArts [43] and FormCalc [44]. The relevant Feynman rules are collected in Table I in Appendix A (for a full set, see Refs. [19–21]).

A. $h \to WW^* \to Wf\bar{f}'$ and $h \to ZZ^* \to Zf\bar{f}$

For these decay amplitudes, we follow a similar presentation as in [29], where these decays were also studied within the HEFT context. We focus in this work on the tree-level amplitudes for these decays. We represent collectively these decay processes as $h \to VV^* \to Vf\bar{f}$, where the EW gauge boson V can be W or Z, and the corresponding Feynman diagram is shown in Fig. 1. The tree-level amplitude can be generically written as

$$\mathcal{A} = \mathcal{A}^\mu \epsilon_\mu^* = (i\Gamma_{hVV}^{\mu\nu})\Delta_{\nu\rho}^{VV}(i\Gamma_{ffV}^\rho)\epsilon_\mu^*, \qquad (4.1)$$

where ϵ_μ^* is the polarization vector of the outgoing on-shell gauge boson, $\Gamma_{hVV}^{\mu\nu}$ is the 1PI with three legs corresponding to hVV, $\Delta_{\nu\rho}^{VV}$ is the gauge boson propagator, and Γ_{ffV}^ρ is the 1PI with three legs corresponding to ffV.

First, it should be noticed that the gauge boson propagator is the same in the three considered models SM, HEFT, and 2HDM. On the other hand, it should also be noticed that the fermion interactions with the gauge bosons are also the same as in the SM. Therefore, the above decay amplitudes differ in each model only on the interaction hVV, which can be read from Table I:

$$i\Gamma_{hVV}^{\mu\nu}|_{\text{SM}} = \frac{2im_V^2}{v}g^{\mu\nu},$$

$$i\Gamma_{hVV}^{\mu\nu}|_{\text{HEFT}} = \frac{2im_V^2}{v}ag^{\mu\nu},$$

$$i\Gamma_{hVV}^{\mu\nu}|_{\text{2HDM}} = \frac{2im_V^2}{v}s_{\beta-\alpha}g^{\mu\nu}. \qquad (4.2)$$

Then, it is clear from the above expressions that the SM is recovered from the HEFT when $a = 1$ (i.e., $\Delta a = 0$) and from the 2HDM in the alignment limit, i.e., for $c_{\beta-\alpha} = 0$, as expected. Notice that, at the tree level, there is no dependence on the heavy Higgs boson masses in these decays.

B. $W^+W^- \to hh$

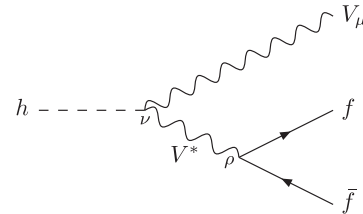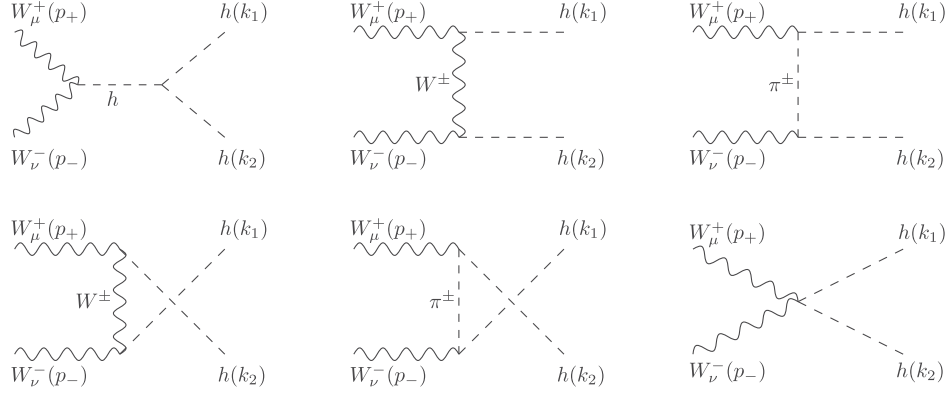Next, we study this WW scattering process at the tree level in the three considered models, SM, HEFT, and

FIG. 1. Generic Feynman diagram for the Higgs decays $h \to VV^* \to Vf\bar{f}$, with $V = W, Z$.

FIG. 2.   Tree-level diagrams contributing to $WW \to hh$ in the SM and the HEFT for arbitrary R_ξ gauge.

2HDM. First, to fix the notation, we set the momenta and Lorentz indices involved in this scattering as follows:

$$W_\mu^+(p_+)W_\nu^-(p_-) \to h(k_1)h(k_2), \qquad (4.3)$$

where $p_\pm$ and $k_{1,2}$ (with $p_+ + p_- = k_1 + k_2$) are the incoming and outgoing momenta, respectively, of the bosons. The $W^\pm$ polarization vectors are $\epsilon_\pm$, respectively. We present the results by separating the contributions from the various scattering channels s, t, u, and contact c channels, since we will compare the different Lorentz structures and energy dependence in our posterior study of the matching equations:

$$\mathcal{A} = \mathcal{A}|_s + \mathcal{A}|_t + \mathcal{A}|_u + \mathcal{A}|_c. \qquad (4.4)$$

Notice that the cancellation of the ξ-dependent terms occurs when the external bosons are taken on shell, and it happens for the t and u channels separately. Furthermore, this cancellation proceeds when adding the two kind of diagrams, with EW gauge boson and GB internal propagators that are present in both the t and u channels. One can also check that the final result for the amplitude of the R_ξ gauges is the same as the result obtained using the unitary gauge (with the W propagator given in the unitary gauge and where no diagrams with GB modes appear in the computation), as expected, since the result of the amplitude must be gauge invariant.

The SM diagrams are shown in Fig. 2, and the resulting amplitude by channels is given by

$$\mathcal{A}^{\text{SM}}|_s = 3g^2 \frac{\lambda v^2}{s - m_h^2} \epsilon_+ \cdot \epsilon_-,$$

$$\mathcal{A}^{\text{SM}}|_t = g^2 \frac{m_W^2 \epsilon_+ \cdot \epsilon_- + \epsilon_+ \cdot k_1 \epsilon_- \cdot k_2}{t - m_W^2},$$

$$\mathcal{A}^{\text{SM}}|_u = g^2 \frac{m_W^2 \epsilon_+ \cdot \epsilon_- + \epsilon_+ \cdot k_2 \epsilon_- \cdot k_1}{u - m_W^2},$$

$$\mathcal{A}^{\text{SM}}|_c = \frac{g^2}{2} \epsilon_+ \cdot \epsilon_-, \qquad (4.5)$$

where $\lambda = m_h^2/(2v^2)$.

Within the HEFT, the diagrams are also collected in Fig. 2, and the result for the amplitude is also gauge invariant. The corresponding LO contributions (i.e., from $\mathcal{L}_2$) from the various channels, at the tree level, are given by

$$\mathcal{A}^{\text{HEFT}}|_s = 3g^2 a\kappa_3 \frac{\lambda v^2}{s - m_h^2} \epsilon_+ \cdot \epsilon_-,$$

$$\mathcal{A}^{\text{HEFT}}|_t = g^2 a^2 \frac{m_W^2 \epsilon_+ \cdot \epsilon_- + \epsilon_+ \cdot k_1 \epsilon_- \cdot k_2}{t - m_W^2},$$

$$\mathcal{A}^{\text{HEFT}}|_u = g^2 a^2 \frac{m_W^2 \epsilon_+ \cdot \epsilon_- + \epsilon_+ \cdot k_2 \epsilon_- \cdot k_1}{u - m_W^2},$$

$$\mathcal{A}^{\text{HEFT}}|_c = \frac{g^2}{2} b\epsilon_+ \cdot \epsilon_-, \qquad (4.6)$$

where again the relation $\lambda = m_h^2/(2v^2)$ is understood.

Regarding the prediction of the amplitude for the 2HDM in covariant R_ξ gauges, we notice that in addition to the
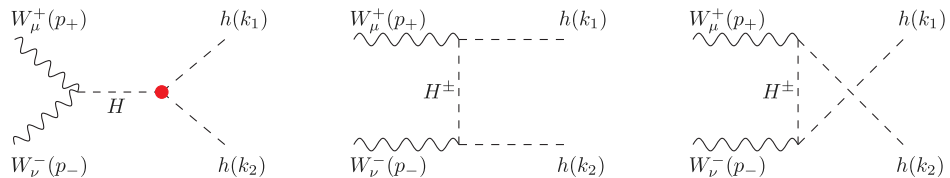
FIG. 3.   Additional tree-level diagrams contributing to $W^+W^- \to hh$ in the 2HDM for arbitrary R_ξ gauge. The triple scalar interaction vertices of the light Higgs with heavy Higgs bosons are denoted with a big dot colored in red.

SM-like diagrams in Fig. 2, where the interchanged Higgs boson is the light Higgs h, there are also the contributions from the exchange of a heavy neutral Higgs boson in the s channel and from the heavy charged Higgs bosons in the t

and u channels, as is shown in Fig. 3. Notice also that the contributions from all these diagrams are ξ independent. And the total result for the amplitude is again gauge invariant. The corresponding amplitudes by channels are

$$\mathcal{A}^{2\mathrm{HDM}}\big|_s = g^2 \left(\frac{3\lambda_{hhh}v^2}{s - m_h^2} s_{\beta-\alpha} + \frac{\lambda_{hhH}v^2}{s - m_H^2} c_{\beta-\alpha} \right) \epsilon_+ \cdot \epsilon_-,$$

$$\mathcal{A}^{2\mathrm{HDM}}\big|_t = g^2 s_{\beta-\alpha}^2 \frac{m_W^2 \epsilon_+ \cdot \epsilon_- + \epsilon_+ \cdot k_1 \epsilon_- \cdot k_2}{t - m_W^2} + g^2 c_{\beta-\alpha}^2 \frac{\epsilon_+ \cdot k_1 \epsilon_- \cdot k_2}{t - m_{H^\pm}^2},$$

$$\mathcal{A}^{2\mathrm{HDM}}\big|_u = g^2 s_{\beta-\alpha}^2 \frac{m_W^2 \epsilon_+ \cdot \epsilon_- + \epsilon_+ \cdot k_2 \epsilon_- \cdot k_1}{u - m_W^2} + g^2 c_{\beta-\alpha}^2 \frac{\epsilon_+ \cdot k_2 \epsilon_- \cdot k_1}{u - m_{H^\pm}^2},$$

$$\mathcal{A}^{2\mathrm{HDM}}\big|_c = \frac{g^2}{2} \epsilon_+ \cdot \epsilon_-. \tag{4.7}$$

In the s channel, we have used the compact notation for the derived triple Higgs couplings λ_{hhh} and λ_{hhH} in Eqs. (3.8) and (3.9).

It is important to remark that the SM predictions of Eq. (4.5) are recovered from the HEFT ones of Eq. (4.6) by taking $a = b = \kappa_3 = 1$ (i.e., for $\Delta a = \Delta b = \Delta \kappa_3 = 0$). On the other hand, we have also checked that the 2HDM results of Eq. (4.7) in the alignment limit (i.e., for $c_{\beta-\alpha} = 0$) coincide with the SM ones. In Sec. V, we will analyze the effect of the heavy Higgs boson masses away from the alignment limit.

C. $ZZ \to hh$

We follow a similar presentation here as in the previous process. The corresponding notation for the momenta in this case is

$$Z_\mu(p_1) Z_\nu(p_2) \to h(k_1) h(k_2), \tag{4.8}$$

where $p_{1,2}$ and $k_{1,2}$ (with $p_1 + p_2 = k_1 + k_2$) are the incoming and outgoing momenta, respectively, of the bosons. The Z polarization vectors are $\epsilon_{1,2}$, respectively. The resulting diagrams in the SM and EChL are collected
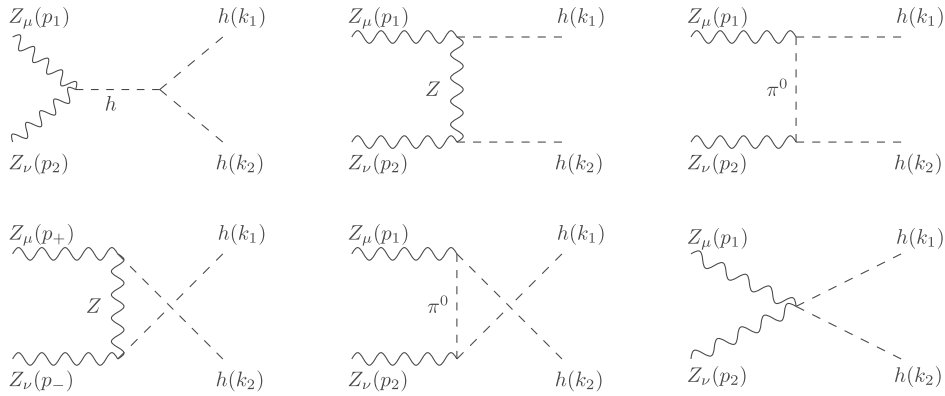

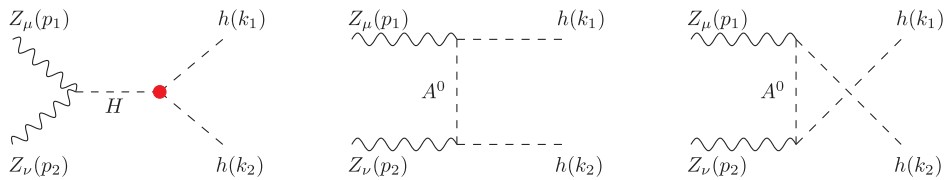FIG. 4. Tree-level diagrams contributing to $ZZ \to hh$ in the SM and the HEFT for arbitrary R_ξ gauge.

FIG. 5. Additional tree-level diagrams contributing to $ZZ \to hh$ in the 2HDM for arbitrary R_ξ gauge. The triple scalar interaction vertices of the light Higgs with heavy Higgs bosons are denoted with a big dot colored in red.

in Fig. 4, and the additional diagrams in the 2HDM are shown in Fig. 5.

Notice that the amplitudes in this case can also be derived from the previous ones by multiplying them by c_w^{-2} and replacing $m_W \to m_Z$ and $m_{H^\pm} \to m_A$. Explicitly, the SM amplitude by channels is

$$\mathcal{A}^{SM}\big|_s = 3\frac{g^2}{c_w^2}\frac{\lambda v^2}{s - m_h^2}\epsilon_1 \cdot \epsilon_2,$$

$$\mathcal{A}^{SM}\big|_t = \frac{g^2}{c_w^2}\frac{m_Z^2\epsilon_1 \cdot \epsilon_2 + \epsilon_1 \cdot k_1\epsilon_2 \cdot k_2}{t - m_Z^2},$$

$$\mathcal{A}^{SM}\big|_u = \frac{g^2}{c_w^2}\frac{m_Z^2\epsilon_1 \cdot \epsilon_2 + \epsilon_1 \cdot k_2\epsilon_2 \cdot k_1}{u - m_Z^2},$$

$$\mathcal{A}^{SM}\big|_c = \frac{g^2}{2c_w^2}\epsilon_1 \cdot \epsilon_2. \tag{4.9}$$

The HEFT amplitude by channels is

$$\mathcal{A}^{HEFT}\big|_s = 3\frac{g^2}{c_w^2}a\kappa_3\frac{\lambda v^2}{s - m_h^2}\epsilon_1 \cdot \epsilon_2,$$

$$\mathcal{A}^{HEFT}\big|_t = \frac{g^2}{c_w^2}a^2\frac{m_Z^2\epsilon_1 \cdot \epsilon_2 + \epsilon_1 \cdot k_1\epsilon_2 \cdot k_2}{t - m_Z^2},$$

$$\mathcal{A}^{HEFT}\big|_u = \frac{g^2}{c_w^2}a^2\frac{m_Z^2\epsilon_1 \cdot \epsilon_2 + \epsilon_1 \cdot k_2\epsilon_2 \cdot k_1}{u - m_Z^2},$$

$$\mathcal{A}^{HEFT}\big|_c = \frac{g^2}{2c_w^2}b\epsilon_1 \cdot \epsilon_2. \tag{4.10}$$

The 2HDM amplitude by channels is

$$\mathcal{A}^{2HDM}\big|_s = \frac{g^2}{c_w^2}\left(\frac{3v^2}{s - m_h^2}\lambda_{hhh}s_{\beta-\alpha} + \frac{v^2}{s - m_H^2}\lambda_{hhH}c_{\beta-\alpha}\right)\epsilon_1 \cdot \epsilon_2,$$

$$\mathcal{A}^{2HDM}\big|_t = \frac{g^2}{c_w^2}s_{\beta-\alpha}^2\frac{m_Z^2\epsilon_1 \cdot \epsilon_2 + \epsilon_1 \cdot k_1\epsilon_2 \cdot k_2}{t - m_Z^2} + \frac{g^2}{c_w^2}c_{\beta-\alpha}^2\frac{\epsilon_1 \cdot k_1\epsilon_2 \cdot k_2}{t - m_A^2},$$

$$\mathcal{A}^{2HDM}\big|_u = \frac{g^2}{c_w^2}s_{\beta-\alpha}^2\frac{m_Z^2\epsilon_1 \cdot \epsilon_2 + \epsilon_1 \cdot k_2\epsilon_2 \cdot k_1}{u - m_Z^2} + \frac{g^2}{c_w^2}c_{\beta-\alpha}^2\frac{\epsilon_1 \cdot k_2\epsilon_2 \cdot k_1}{u - m_A^2},$$

$$\mathcal{A}^{2HDM}\big|_c = \frac{g^2}{2c_w^2}\epsilon_1 \cdot \epsilon_2. \tag{4.11}$$

In particular, the SM results are also recovered from the HEFT ones when $a = b = \kappa_3 = 1$ (i.e., for $\Delta a = \Delta b = \Delta\kappa_3 = 0$) and from the 2HDM in the alignment limit (i.e., for $c_{\beta-\alpha} = 0$).

D. $hh \to hh$

The tree-level diagrams contributing in the SM and the HEFT are the same set and are collected in Fig. 6. In the case of the 2HDM, these four diagrams in Fig. 6 also contribute, and besides them there are also diagrams where the heavy neutral Higgs boson propagates in the s, t, and u channels. These additional diagrams are collected in Fig. 7. It should be noted that all these diagrams are independent of the ξ gauge parameter, and, therefore, the results for the amplitudes in the three models are gauge invariant, as expected.
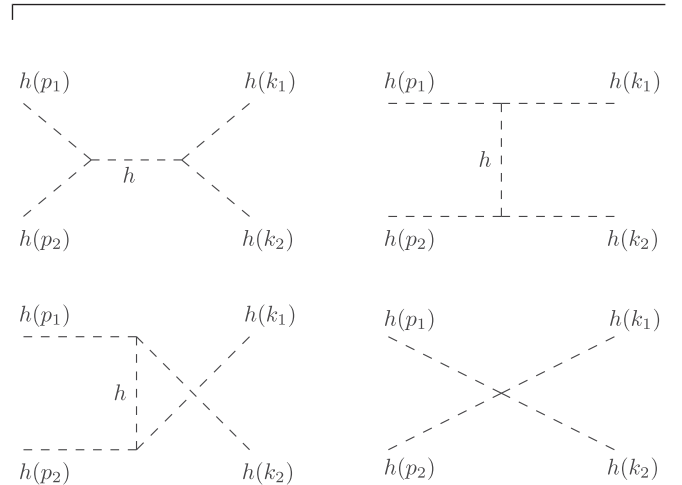

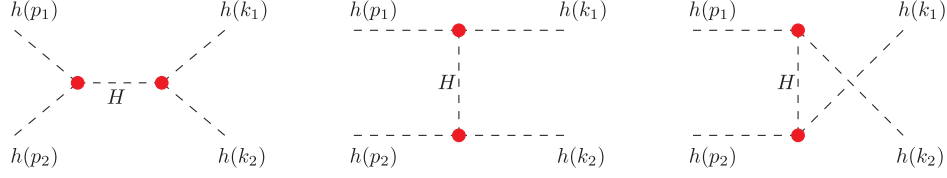FIG. 6. Tree-level diagrams contributing to $hh \to hh$ in the SM and in the HEFT for arbitrary R_ξ gauge.

FIG. 7. Additional tree-level diagrams contributing to $hh \to hh$ in the 2HDM for arbitrary R_ξ gauge. The triple scalar interaction vertices of the light Higgs with heavy Higgs bosons are denoted with a big dot colored in red.

The SM amplitude by channels is

$$\mathcal{A}^{\mathrm{SM}}|_s = -\frac{36\lambda^2 v^2}{s - m_h^2},$$

$$\mathcal{A}^{\mathrm{SM}}|_t = -\frac{36\lambda^2 v^2}{t - m_h^2},$$

$$\mathcal{A}^{\mathrm{SM}}|_u = -\frac{36\lambda^2 v^2}{u - m_h^2},$$

$$\mathcal{A}^{\mathrm{SM}}|_c = -6\lambda, \tag{4.12}$$

where, again, $\lambda = m_h^2/(2v^2)$.

The HEFT amplitude by channels is

$$\mathcal{A}^{\mathrm{HEFT}}|_s = -\frac{36\lambda^2 v^2}{s - m_h^2}\kappa_3^2,$$

$$\mathcal{A}^{\mathrm{HEFT}}|_t = -\frac{36\lambda^2 v^2}{t - m_h^2}\kappa_3^2,$$

$$\mathcal{A}^{\mathrm{HEFT}}|_u = -\frac{36\lambda^2 v^2}{u - m_h^2}\kappa_3^2,$$

$$\mathcal{A}^{\mathrm{HEFT}}|_c = -6\lambda\kappa_4. \tag{4.13}$$

The 2HDM amplitude by channels is

$$\mathcal{A}^{\mathrm{2HDM}}|_s = -\frac{36v^2}{s - m_h^2}\lambda_{hhh}^2 - \frac{4v^2}{s - m_H^2}\lambda_{hhH}^2,$$

$$\mathcal{A}^{\mathrm{2HDM}}|_t = -\frac{36v^2}{t - m_h^2}\lambda_{hhh}^2 - \frac{4v^2}{t - m_H^2}\lambda_{hhH}^2,$$

$$\mathcal{A}^{\mathrm{2HDM}}|_u = -\frac{36v^2}{u - m_h^2}\lambda_{hhh}^2 - \frac{4v^2}{u - m_H^2}\lambda_{hhH}^2,$$

$$\mathcal{A}^{\mathrm{2HDM}}|_c = -6\lambda_{hhhh}, \tag{4.14}$$

where the derived values for the triple λ_{hhh}, λ_{hhH}, and quartic λ_{hhhh} couplings are given in Eqs. (3.8), (3.9), and (3.11), respectively.

As in the previous observables, the SM results are recovered from the HEFT ones for $\kappa_3 = \kappa_4 = 1$ (i.e., for $\Delta\kappa_3 = \Delta\kappa_4 = 0$) and from the 2HDM in the alignment limit (i.e., for $c_{\beta-\alpha} = 0$).

E. $h \to \gamma\gamma$

This decay occurs at one-loop level in the three considered models; thus, the predictions for their corresponding amplitudes are all of $\mathcal{O}(\hbar/(16\pi^2))$. The computation of this observable in R_ξ covariant gauges was presented in [45] for the SM and in [22] for the HEFT, where it was also recomputed the SM case, for comparison. In this presentation, we follow the computation as described in [22].

In the SM case, when adding all the one-loop diagrams in the R_ξ gauges given in Fig. 8, the total one-loop amplitude is UV finite and does not need renormalization nor counterterms. The ξ-dependence cancellation among the various loop diagrams, leading to the gauge invariance of the resulting one-loop amplitude, was also fully discussed in [22]. Notice that, for the purpose of the present work where we are interested only in the bosonic part of the models, we do not need to compute the loops with fermions.

The result of the SM one-loop amplitude for the decay $h(q) \to \gamma(k_1)\gamma(k_2)$ in covariant R_ξ gauges respects the Lorentz structure expected by the $U(1)$ Ward identity and can be written as

$$\mathcal{A}^{\mathrm{SM}}(h \to \gamma\gamma) = \frac{1}{v}F_{h\gamma\gamma}(m_h^2(\epsilon_1\epsilon_2) - 2(\epsilon_1 k_2)(\epsilon_2 k_1)), \tag{4.15}$$

where the explicit computation of all the bosonic loops gives

$$F_{h\gamma\gamma} = \frac{g^2 s_w^2}{8\pi^2 m_h^2}\left(12\frac{m_W^2}{m_h^2}(m_h^2 - 2m_W^2)f\left(\frac{4m_W^2}{m_h^2}\right) + m_h^2 + 6m_W^2\right). \tag{4.16}$$

The definition of the one-loop function $f(r)$ in the above formula is given in Appendix B. The result has also been checked to be the same when computing the loop contributions to the amplitude in the unitary gauge (see also [22]).

For the HEFT case, the same one-loop diagrams displayed in Fig. 8 contribute to the decay amplitude but with different values than in the SM. Recall that the Feynman rules in both theories are different. In particular, the ghost diagrams are absent within the HEFT (i.e., diagram 3 in this figure vanishes) due to the vanishing couplings of the h with the ghosts in this nonlinear theory (see Ref. [22] for
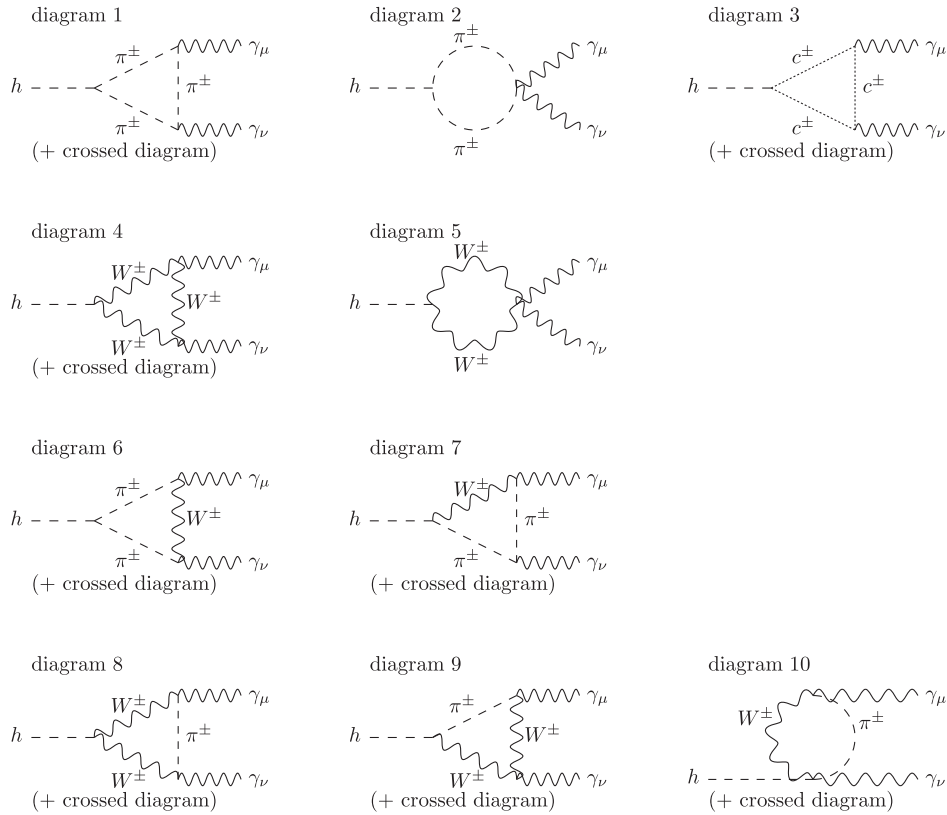
FIG. 8. Bosonic one-loop diagrams contributing to $h \to \gamma\gamma$ within the SM in covariant R_ξ gauges. In the HEFT case, these one-loop diagrams also contribute to the amplitude. The contributions from these diagrams are different in the SM and HEFT cases. In the 2HDM case, these one-loop diagrams also contribute but again with different values than in the SM and in the HEFT. Within the HEFT, there are additional diagrams as summarized in Fig. 9. Within the 2HDM, there are additional diagrams as summarized in Fig. 10.

details and also for the interesting comparison between the computation in the covariant gauges and the unitary gauge). The additional diagrams in the HEFT are represented in Fig. 9. All the loop diagrams come from $\mathcal{L}_2$ in Eq. (2.5) and the tree-level contribution comes from the $\mathcal{L}_4$ in Eq. (2.9). Diagrams (a) and (b) appear in the HEFT due to the nonlinear representation for the GBs that provide new couplings for them that are not present in the SM. Diagram (c) appears due to the tree-level contributions from the effective operators in $\mathcal{L}_4$ which provide a term in the decay amplitude involving the effective coefficient $a_{h\gamma\gamma}$. It is interesting to recall that the sum all the one-loop diagrams in the HEFT gives also a UV finite result. This means that $a_{h\gamma\gamma}$ does not need to be renormalized; i.e., in this h decay,

the relevant coefficient in $\mathcal{L}_4$ does not need to act as a counterterm for the loops from $\mathcal{L}_2$, since they provide a finite result.

The result of the HEFT amplitude for this decay is

$$
\begin{aligned}
\mathcal{A}^{\text{HEFT}}(h \to \gamma\gamma) &= \mathcal{A}^{\mathcal{L}_2^{\text{loop}}} + \mathcal{A}^{\mathcal{L}_4^{\text{tree}}} \\
&= \frac{1}{v}(aF_{h\gamma\gamma} + g^2 s_{\text{w}}^2 a_{h\gamma\gamma}) \\
&\quad \times (m_h^2(\epsilon_1\epsilon_2) - 2(\epsilon_1 k_2)(\epsilon_2 k_1)),
\end{aligned}
$$

(4.17)

where $aF_{h\gamma\gamma}$ collects the contributions from the loops computed with $\mathcal{L}_2$ and the term proportional to $a_{h\gamma\gamma}$ corresponds to the tree-level contribution from $\mathcal{L}_4$.
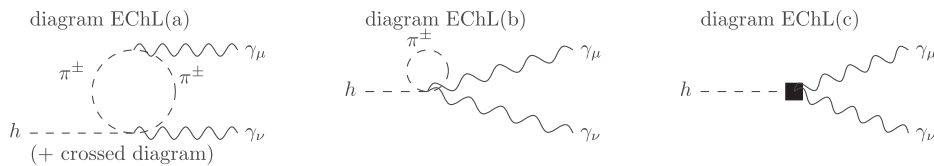

FIG. 9. Additional diagrams contributing to $h \to \gamma\gamma$ in the HEFT for arbitrary R_ξ gauge. The black box represents the contribution from $a_{h\gamma\gamma}$ in $\mathcal{L}_4$.
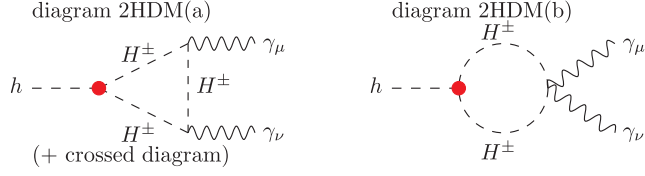
FIG. 10. Additional diagrams contributing to $h \to \gamma\gamma$ in the 2HDM for arbitrary R_ξ gauge. The triple scalar interaction vertices of the light Higgs with heavy Higgs bosons are denoted with a big dot colored in red.

FIG. 11. Additional diagrams contributing to $h \to \gamma Z$ that are not present in $h \to \gamma\gamma$. The black box represents the tree-level contribution of the counterterms. The big black ball represents the renormalized two-point 1PI γZ function.

The computation of the one-loop amplitude in the 2HDM case for the generic R_ξ gauges involves the computation [6,46] of the one-loop diagrams in Fig. 8 and the additional one-loop diagrams in Fig. 10. We have checked that the sum of all loops are ξ independent. Notice that these additional diagrams correspond to the one-loop contributions involving the charged Higgs bosons in the internal propagators and are ξ independent. We have checked that after adding all the loop diagrams the result is also ξ independent. The resulting amplitude (bosonic contributions) within the 2HDM is the following:

$$\mathcal{A}^{\text{2HDM}}(h \to \gamma\gamma) = \frac{1}{v}(s_{\beta-\alpha}F_{h\gamma\gamma} + F_{h\gamma\gamma}^{H^\pm})$$
$$\times (m_h^2(\epsilon_1\epsilon_2) - 2(\epsilon_1 k_2)(\epsilon_2 k_1)), \quad (4.18)$$

where $s_{\beta-\alpha}F_{h\gamma\gamma}$ corresponds to the diagrams in Fig. 8 and $F_{h\gamma\gamma}^{H^\pm}$ is the extra contribution from the $H^\pm$ loops in Fig. 10. This latter is given by

$$F_{h\gamma\gamma}^{H^\pm} = \frac{g^2 v^2 \lambda_{hH^+H^-} s_w^2}{8\pi^2 m_h^2}\left(1 - \frac{4m_{H^\pm}^2}{m_h^2}f\left(\frac{4m_{H^\pm}^2}{m_h^2}\right)\right). \quad (4.19)$$

Again, the function $f(r)$ is given in Appendix B. An important point to remark here is that $F_{h\gamma\gamma}^{H^\pm}$ depends on the
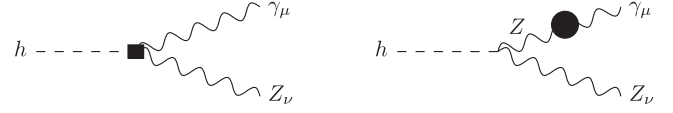
triple coupling $\lambda_{hH^+H^-}$ whose derived value in terms of the input parameters is given in Eq. (3.10).

F. $h \to \gamma Z$

The computation of the decay amplitude in the $h \to \gamma Z$ is similar to the previous $h \to \gamma\gamma$ case (with slight differences commented below), and it was also presented in [22] for arbitrary R_ξ gauge within both SM and HEFT. We recall here just the most relevant points. The main set of one-loop diagrams in the SM are the same as in Fig. 8 replacing one photon by a Z boson. In this case, however, the sum of all the one-loop diagrams in this figure is not UV convergent, and the contributions in Fig. 11 must be included in order to get a UV finite and ξ-independent amplitude respecting the Ward identity. In particular, we include the counterterm of the three-leg 1PI Green function (left diagram in Fig. 11) and the loop and counterterm contributions yielding to the two-leg renormalized 1PI self-energy photon-Z (represented by the black ball in the right diagram of this figure).

The result of the SM one-loop amplitude (bosonic contributions) for $h(q) \to \gamma(k_1)Z(k_2)$ in a R_ξ gauge is the following:

$$\mathcal{A}^{\text{SM}}(h \to \gamma Z) = \frac{1}{v}F_{h\gamma Z}((m_h^2 - m_Z^2)(\epsilon_1\epsilon_2) - 2(\epsilon_1 k_2)(\epsilon_2 k_1)), \quad (4.20)$$

where

$$F_{h\gamma Z} = \frac{g^2 s_w c_w}{16\pi^2(m_h^2 - m_Z^2)}\left(2m_h^2 + 12m_W^2 - \frac{m_Z^2}{m_W^2}m_h^2 - 2m_Z^2\right.$$
$$- \frac{4m_W^2}{m_h^2 - m_Z^2}\left(-6m_h^2 + 12m_W^2 + \frac{m_Z^2}{m_W^2}m_h^2 + 6m_Z^2 - \frac{2m_Z^4}{m_W^2}\right)\left(f\left(\frac{4m_W^2}{m_h^2}\right) - f\left(\frac{4m_W^2}{m_Z^2}\right)\right)$$
$$\left. - \frac{2m_Z^2}{m_h^2 - m_Z^2}\left(2m_h^2 + 12m_W^2 - \frac{m_Z^2}{m_W^2}m_h^2 - 2m_Z^2\right)\left(g\left(\frac{4m_W^2}{m_h^2}\right) - g\left(\frac{4m_W^2}{m_Z^2}\right)\right)\right). \quad (4.21)$$

The definitions of the one-loop functions $f(r)$ and $g(r)$ are given in Appendix B.

The result of the HEFT one-loop amplitude (bosonic contributions) for $h(q) \to \gamma(k_1)Z(k_2)$ in a R_ξ gauge is the following:

$$\mathcal{A}^{\text{HEFT}}(h \to \gamma Z) = \mathcal{A}^{\mathcal{L}_2^{\text{loop}}} + \mathcal{A}^{\mathcal{L}_4^{\text{tree}}} = \frac{1}{v}(aF_{h\gamma Z} + g^2 s_w c_w a_{h\gamma Z})((m_h^2 - m_Z^2)(\epsilon_1\epsilon_2) - 2(\epsilon_1 k_2)(\epsilon_2 k_1)), \quad (4.22)$$

where $aF_{h\gamma Z}$ summarizes the one-loop contributions from $\mathcal{L}_2$ and the term proportional to $a_{h\gamma Z}$ comes from $\mathcal{L}_4$ at the tree level. In this case, the coefficient $a_{h\gamma Z}$ also acts as counterterm.

The result of the 2HDM one-loop amplitude [6,46] (bosonic contributions) for $h(q) \to \gamma(k_1)Z(k_2)$ in a R_ξ gauge is the following:

$$\mathcal{A}^{2\text{HDM}}(h \to \gamma Z) = \frac{1}{v}(s_{\beta-\alpha}F_{h\gamma Z} + F_{h\gamma Z}^{H^\pm})((m_h^2 - m_Z^2)(\epsilon_1\epsilon_2) - 2(\epsilon_1 k_2)(\epsilon_2 k_1)), \qquad (4.23)$$

where $s_{\beta-\alpha}F_{h\gamma Z}$ comes from the one-loop diagrams and counterterms already present in the SM and $F_{h\gamma Z}^{H^\pm}$ is the additional contribution from the $H^\pm$ loops:

$$F_{h\gamma Z}^{H^\pm} = \frac{\lambda_{hH^+H^-}s_\text{w}c_\text{w}(2m_W^2 - m_Z^2)}{4\pi^2(m_h^2 - m_Z^2)^2}\left(m_h^2 - m_Z^2 - 2m_Z^2\left(g\left(\frac{4m_{H^\pm}^2}{m_h^2}\right) - g\left(\frac{4m_{H^\pm}^2}{m_Z^2}\right)\right)\right.$$

$$\left. -m_{H^\pm}^2\log^2\left(\frac{2m_{H^\pm}^2 - m_Z^2 + \sqrt{-m_Z^2(4m_{H^\pm}^2 - m_Z^2)}}{2m_{H^\pm}^2}\right) + m_{H^\pm}^2\log^2\left(\frac{2m_{H^\pm}^2 - m_h^2 + \sqrt{-m_h^2(4m_{H^\pm}^2 - m_h^2)}}{2m_{H^\pm}^2}\right)\right). \qquad (4.24)$$

Once again, this contribution is proportional to the triple coupling of the light Higgs with the charged Higgs bosons Eq. (3.10).

V. MATCHING HEFT AND 2HDM AMPLITUDES

In this section, we first set the matching equations relating the HEFT and the 2HDM amplitudes, and, second, we solve these equations analytically providing the solutions for the HEFT coefficients in terms of the 2HDM input parameters. First, we define this matching by equating the amplitudes from the HEFT with the amplitudes from the 2HDM in the heavy Higgs bosons limit. This heavy Higgs boson limit refers to consider heavy H, A, and $H^\pm$ with respect to the EW scale v or, equivalently, respect to all EW masses involved: $m_H, m_A, m_{H^\pm} \gg m_W, m_Z, m_h, v, m_{12}$. In the case of scattering amplitudes, by heavy BSM Higgs boson limit, we also mean heavy with respect to the energy of the scattering process, i.e., $m_\text{heavy} \gg \sqrt{s}$, where m_heavy denotes collectively any of the heavy masses involved, m_H, m_A, and $m_{H^\pm}$. Thus, for shortness, in the following, we will refer generically to this large heavy mass limit by requiring a big hierarchy among the two scales, i.e., by considering

$$m_\text{heavy} \gg m_\text{EW}, \qquad (5.1)$$

where, generically, we are assuming that m_heavy is closer to the TeV scale and m_EW, the masses and energies involved, is closer to the EW scale. Then, for a given amplitude $\mathcal{A}$ our generic matching condition reads as follows:

$$\mathcal{A}^\text{HEFT} = \mathcal{A}_\text{heavy}^\text{2HDM}, \qquad (5.2)$$

where $\mathcal{A}^\text{HEFT}$ is the prediction from the HEFT and $\mathcal{A}_\text{heavy}^\text{2HDM}$ means the result of the 2HDM amplitude after integrating out the heavy modes. This integration is performed in practice by means of an expansion of the 2HDM amplitude in inverse powers of the heavy boson masses. Generically, this large mass expansion will lead to terms in the total amplitude with increasing powers in a small mass ratio, namely, with increasing orders in $\sim(m_\text{EW}^2/m_\text{heavy}^2)^n$ with $n = 0, 2, 4, \dots$. On the other hand, this matching condition can be set at any order in the loop expansion, i.e., to $\mathcal{O}(\hbar^0)$, $\mathcal{O}(\hbar^1)$, etc., but in any case this order must be fixed equally in both sizes of the matching equations. Correspondingly, the solutions to the matching equations will be provided at a fixed order, i.e., either at the tree level or at the one-loop level, etc. Finally, since we are mainly interested in capturing the nondecoupling effects from the heavy Higgs bosons, encoded in those solutions, we will need to focus only on the leading terms of this large mass expansion. Therefore, we will keep in this work only those leading terms in $\mathcal{A}_\text{heavy}^\text{2HDM}$ that go with the $n = 0$ power or, equivalently, the contributions which are constant with the heavy mass m_heavy in the heavy mass limit. As we will see, there are no contributions with negative n; i.e., the total result of the amplitude never grows with the heavy masses, thus demonstrating that the large mass expansion is convergent. The final comment regarding the previous matching equation is that, when solving it, we must write the solutions for BSM with respect to the SM ones. This is equivalent to saying that the solutions of the matching equations at the leading order in the large mass expansion must be provided at the end for Δa, Δb, $\Delta\kappa_3$, $\Delta\kappa_4$, $a_{h\gamma\gamma}$, and $a_{h\gamma Z}$, and these must be given in terms of the input parameters

(other than the heavy masses) of the 2HDM, namely, in terms of v, m_h, $c_{\beta-\alpha}$, t_β, and m_{12}, as set in Eq. (3.3).

Our matching procedure systematically solves the above Eq. (5.2) by taking into account all the Lorentz structures involved and considering both the energy and scattering angle dependencies of the scattering amplitudes $\mathcal{A} = \mathcal{A}(s, \theta)$ (or masses and momenta dependence in the case of decay amplitudes). Then we solve the matching conditions sequentially and process by process. In this matching, we consider the full set of seven amplitudes presented in the previous section. Notice that some HEFT coefficients are present in various amplitudes; therefore, once we solve them from one subset of amplitudes, the remaining ones are used to cross-check the results. This is useful to check that our solutions for the HEFT coefficients in terms of the 2HDM input parameters are the same for all the considered processes, and, therefore, they are process-independent results.

A. Amplitudes for large m_{heavy} in the 2HDM and solutions to the matching

As announced above, we keep here just the dominant contributions in the large m_{heavy} expansion that define the nondecoupling effects from the heavy modes, which for the selected amplitudes here correspond to the resulting contributions that are independent of the heavy Higgs boson masses; i.e., they behave as $(m_{\text{EW}}/m_{\text{heavy}})^0$. The next-to-leading terms in these expansions are decoupling, going as

$(m_{\text{EW}}/m_{\text{heavy}})^n$ with $n = 2, 4, \ldots$, etc., and are not included in our solutions to the matching equations. In the computation of this expansion, it is crucial to take into account that λ_{hhH}, $\lambda_{hH^+H^-}$, and λ_{hhhh} depend on the heavy masses of the BSM Higgs bosons as it is shown in Eqs. (3.9)–(3.11). Another important point to take into account is that, due to the previously shown ξ independence of the separate contributions to the amplitudes from the various channels s, t, u, and c, the matching equations can be analyzed by channels.

1. $h \to VV^* \to Vf\bar{f}$

The starting matching equation is for the decay amplitudes of the light Higgs boson into a gauge boson W or Z and a fermion pair, at the tree level. The solution of the matching equation in this case is trivial, since the 2HDM amplitude does not depend on m_{heavy}. Therefore, the solution to the matching equation in these two decays gives simply

$$a = 1 - \Delta a = s_{\beta-\alpha}. \tag{5.3}$$

2. $W^+W^- \to hh$

The next matching equation is for the $W^+W^- \to hh$ scattering. In this case, the large heavy mass expansion gives the following results for the 2HDM amplitude, presented here by channels:

$$
\begin{aligned}
\mathcal{A}_{\text{heavy}}^{\text{2HDM}}|_s &= g^2 \left(\frac{3s_{\beta-\alpha}}{s - m_h^2} \left(s_{\beta-\alpha}(1 + 2c_{\beta-\alpha}^2)\frac{m_h^2}{2} - s_{\beta-\alpha}c_{\beta-\alpha}^2 \frac{m_{12}^2}{s_\beta c_\beta} + c_{\beta-\alpha}^3 \cot 2\beta \left(m_h^2 - \frac{m_{12}^2}{s_\beta c_\beta} \right) \right) \right. \\
&\quad \left. - \frac{c_{\beta-\alpha}^2}{2}(-2c_{\beta-\alpha}s_{\beta-\alpha} \cot 2\beta + 2c_{\beta-\alpha}^2 - 1) \right) \epsilon_+ \cdot \epsilon_-, \\
\mathcal{A}_{\text{heavy}}^{\text{2HDM}}|_t &= g^2 s_{\beta-\alpha}^2 \frac{m_W^2 \epsilon_+ \cdot \epsilon_- + \epsilon_+ \cdot k_1 \epsilon_- \cdot k_2}{t - m_W^2}, \\
\mathcal{A}_{\text{heavy}}^{\text{2HDM}}|_u &= g^2 s_{\beta-\alpha}^2 \frac{m_W^2 \epsilon_+ \cdot \epsilon_- + \epsilon_+ \cdot k_2 \epsilon_- \cdot k_1}{u - m_W^2}, \\
\mathcal{A}_{\text{heavy}}^{\text{2HDM}}|_c &= \frac{g^2}{2} \epsilon_+ \cdot \epsilon_-.
\end{aligned}
\tag{5.4}
$$

By comparing first the t and u channels in Eq. (4.6) with those in Eq. (5.4), we confirm the previous solution for a in Eq. (5.3). Second, by comparing the contact channel in Eq. (4.6) with the s-independent contribution of the s-channel and the contact channel in Eq. (5.4), we arrive to

$$b = 1 - \Delta b = 1 + c_{\beta-\alpha}^2(1 - 2c_{\beta-\alpha}^2 + 2c_{\beta-\alpha}s_{\beta-\alpha} \cot 2\beta). \tag{5.5}$$

Finally, by plugging the previous solution for a in Eq. (5.3) in the s channel in Eq. (4.6) and comparing it with the s-dependent contribution of the s channel in Eq. (5.4), we find

$$\kappa_3 = 1 - \Delta\kappa_3 = s_{\beta-\alpha}(1 + 2c_{\beta-\alpha}^2) + c_{\beta-\alpha}^2 \left(-2s_{\beta-\alpha}\frac{m_{12}^2}{m_h^2 s_\beta c_\beta} + 2c_{\beta-\alpha} \cot 2\beta \left(1 - \frac{m_{12}^2}{m_h^2 s_\beta c_\beta} \right) \right). \tag{5.6}$$

3. $ZZ \to hh$

The procedure here is similar to in the previous WW scattering. From Eq. (4.11), we get the following large heavy mass expansion results for the 2HDM amplitude, presented again by channels:

$$
\mathcal{A}_{\text{heavy}}^{\text{2HDM}}\big|_s = \frac{g^2}{c_{\text{w}}^2}\left(\frac{3s_{\beta-\alpha}}{s - m_h^2}\left(s_{\beta-\alpha}(1 + 2c_{\beta-\alpha}^2)\frac{m_h^2}{2} - s_{\beta-\alpha}c_{\beta-\alpha}^2\frac{m_{12}^2}{s_\beta c_\beta} + c_{\beta-\alpha}^3 \cot 2\beta\left(m_h^2 - \frac{m_{12}^2}{s_\beta c_\beta}\right)\right)\right.
$$
$$
\left. - \frac{c_{\beta-\alpha}^2}{2}(-2c_{\beta-\alpha}s_{\beta-\alpha}\cot 2\beta + 2c_{\beta-\alpha}^2 - 1)\right)\epsilon_1 \cdot \epsilon_2,
$$

$$
\mathcal{A}_{\text{heavy}}^{\text{2HDM}}\big|_t = \frac{g^2}{c_{\text{w}}^2}s_{\beta-\alpha}^2\frac{m_W^2\epsilon_1 \cdot \epsilon_2 + \epsilon_1 \cdot k_1 \epsilon_2 \cdot k_2}{t - m_W^2},
$$

$$
\mathcal{A}_{\text{heavy}}^{\text{2HDM}}\big|_u = \frac{g^2}{c_{\text{w}}^2}s_{\beta-\alpha}^2\frac{m_W^2\epsilon_1 \cdot \epsilon_2 + \epsilon_1 \cdot k_2 \epsilon_2 \cdot k_1}{u - m_W^2},
$$

$$
\mathcal{A}_{\text{heavy}}^{\text{2HDM}}\big|_c = \frac{g^2}{2c_{\text{w}}^2}\epsilon_1 \cdot \epsilon_2. \tag{5.7}
$$

By comparing the amplitudes from the HEFT in Eq. (4.10) with the previous 2HDM results and by solving the matching equations in this $ZZ \to hh$ case, we arrive at the same results as Eqs. (5.3)–(5.6). Therefore, this channel serves as a cross-check of the previous solutions.

4. $hh \to hh$

For the case of $hh \to hh$ scattering, the results from Eq. (4.14) in the large heavy mass limit are given by the following expressions, also presented by channels:

$$
\mathcal{A}_{\text{heavy}}^{\text{2HDM}}\big|_s = -\frac{36}{v^2(s - m_h^2)}\left(s_{\beta-\alpha}(1 + 2c_{\beta-\alpha}^2)\frac{m_h^2}{2} - s_{\beta-\alpha}c_{\beta-\alpha}^2\frac{m_{12}^2}{s_\beta c_\beta} + c_{\beta-\alpha}^3\cot 2\beta\left(m_h^2 - \frac{m_{12}^2}{s_\beta c_\beta}\right)\right)^2
$$
$$
+ \frac{m_H^2}{v^2}c_{\beta-\alpha}^2(2c_{\beta-\alpha}^2 - 1 - 2c_{\beta-\alpha}s_{\beta-\alpha}\cot 2\beta)^2
$$
$$
+ \frac{2c_{\beta-\alpha}}{v^2}(2c_{\beta-\alpha}^2 - 1 - 2c_{\beta-\alpha}s_{\beta-\alpha}\cot 2\beta)\left(s\frac{c_{\beta-\alpha}}{2}(2c_{\beta-\alpha}^2 - 1 - 2c_{\beta-\alpha}s_{\beta-\alpha}\cot 2\beta)\right.
$$
$$
+ m_h^2 + c_{\beta-\alpha}^2\left(-4s_{\beta-\alpha}^2\frac{m_{12}^2}{s_\beta c_\beta} + 4c_{\beta-\alpha}^2\cot^2 2\beta\left(-\frac{m_{12}^2}{s_\beta c_\beta} + c_{\beta-\alpha}^2 m_h^2\right)\right.
$$
$$
\left.\left. + 4c_{\beta-\alpha}s_{\beta-\alpha}\cot 2\beta\left(-2\frac{m_{12}^2}{s_\beta c_\beta} + (2c_{\beta-\alpha}^2 + 1)m_h^2\right) - 4c_{\beta-\alpha}^4 m_h^2 + 3m_h^2\right)\right),
$$

$$
\mathcal{A}_{\text{heavy}}^{\text{2HDM}}\big|_t = \mathcal{A}_{\text{heavy}}^{\text{2HDM}}\big|_s \quad \text{with} \quad s \to t,
$$

$$
\mathcal{A}_{\text{heavy}}^{\text{2HDM}}\big|_u = \mathcal{A}_{\text{heavy}}^{\text{2HDM}}\big|_s \quad \text{with} \quad s \to u,
$$

$$
\mathcal{A}_{\text{heavy}}^{\text{2HDM}}\big|_c = -3\frac{m_H^2}{v^2}c_{\beta-\alpha}^2(2c_{\beta-\alpha}^2 - 1 - 2c_{\beta-\alpha}s_{\beta-\alpha}\cot 2\beta)^2 - \frac{3}{v^2}\left(4c_{\beta-\alpha}^3 s_{\beta-\alpha}\cot 2\beta\left((1 + 2c_{\beta-\alpha}^2)m_h^2 - 2\frac{m_{12}^2}{s_\beta c_\beta}\right)\right.
$$
$$
\left. -(-1 + c_{\beta-\alpha}^2)\left((1 + 2c_{\beta-\alpha}^2)^2 m_h^2 - 4c_{\beta-\alpha}^2\frac{m_{12}^2}{s_\beta c_\beta}\right) + 4\cot^2 2\beta\left(c_{\beta-\alpha}^6 m_h^2 - c_{\beta-\alpha}^4\frac{m_{12}^2}{s_\beta c_\beta}\right)\right). \tag{5.8}
$$

Notice the m_H^2 dependence in the separate contributions from the various channels. In this particular case with scalar particles in all the external legs, the result is not organized in different Lorentz structures that can be compared in solving the matching. Thus, the matching cannot be analyzed separately by channels, and it must be done instead by using the total sum; i.e., the matching quantity is the total amplitude. Then, when adding the contributions

from all the channels, one finds that the potentially growing terms with the heavy mass of $\mathcal{O}(m_H^2)$ in the separate contributions are totally canceled in the sum. We have checked this cancellation explicitly in the total amplitude. Thus, the leading dependence on the heavy mass of the total amplitude, after the integration of the heavy modes, is again of $\mathcal{O}(m_{\text{EW}}^2/m_{\text{heavy}}^2)^0$, providing nondecoupling contributions that are constant with m_{heavy}.

In addition, the growing energy behavior in the contributions from the separate s, t, and u channels also disappear in the total amplitude after summing over them using the relation $s + t + u = 4m_h^2$. The resulting total amplitude has contributions decreasing with the s, t, and u variables, and, comparing them with the corresponding HEFT contributions of Eq. (4.13), we arrive to the same solution for κ_3 as obtained previously in Eq. (5.6). Thus, this part serves as a cross-check for κ_3. Finally, by solving the matching equation looking at the contribution to the total amplitude that is constant in energy, one gets the following result for κ_4:

$$
\begin{aligned}
\kappa_4 = 1 - \Delta\kappa_4 = 1 + \frac{c_{\beta-\alpha}^2}{3}\Bigg(&-7 + 64c_{\beta-\alpha}^2 - 76c_{\beta-\alpha}^4 + 12(1 - 6c_{\beta-\alpha}^2 + 6c_{\beta-\alpha}^4)\frac{m_{12}^2}{m_h^2 s_\beta c_\beta} \\
&+ 4c_{\beta-\alpha}s_{\beta-\alpha}\cot 2\beta\left(-13 + 38c_{\beta-\alpha}^2 - 3(-5 + 12c_{\beta-\alpha}^2)\frac{m_{12}^2}{m_h^2 s_\beta c_\beta}\right) \\
&+ 4c_{\beta-\alpha}^2\cot^2 2\beta\left(3c_{\beta-\alpha}^2 - 16s_{\beta-\alpha}^2 + 3(-1 + 6s_{\beta-\alpha}^2)\frac{m_{12}^2}{m_h^2 s_\beta c_\beta}\right)\Bigg).
\end{aligned}
\tag{5.9}
$$

5. $h \to \gamma\gamma$ and $h \to \gamma Z$

Finally, for the Higgs boson decays $h \to \gamma\gamma$ and $h \to \gamma Z$, the results for the one-loop amplitude summarizing the heavy mass limit of the charged Higgs boson loops are obtained from Eqs. (4.19) and (4.24) and by taking into account the large mass behavior of the functions $f(r)$ and $g(r)$ given in Eq. (B7). The results for the functions defining those amplitudes are the following:

$$
\begin{aligned}
F_{h\gamma\gamma}^{H^\pm}\Big|_{\text{heavy}} &= -\frac{g^2 s_w^2 s_{\beta-\alpha}}{48\pi^2}, \\
F_{h\gamma Z}^{H^\pm}\Big|_{\text{heavy}} &= -\frac{g^2 s_w(2c_w^2 - 1)s_{\beta-\alpha}}{96c_w\pi^2}.
\end{aligned}
\tag{5.10}
$$

Plugging these results into the respective matching equations, we finally find the solutions for the HEFT coefficients:

$$
\begin{aligned}
a_{h\gamma\gamma} &= -\frac{s_{\beta-\alpha}}{48\pi^2}, \\
a_{h\gamma Z} &= -\frac{(2c_w^2 - 1)s_{\beta-\alpha}}{96c_w^2\pi^2}.
\end{aligned}
\tag{5.11}
$$

In addition, these decay channels also confirm the solution for a given in Eq. (5.3). Notice that these two coefficients do not vanish in the alignment limit; therefore, they may have relevant phenomenological implications. In particular, the implications of the nondecoupling $H^\pm$ loops in BR($h \to \gamma\gamma$) have been recently analyzed in the context of the LHC physics in [47], and they find sizable departures with respect to the SM rates, even for large $m_{H^\pm}$ near the TeV. Other nondecoupling effects in the 2HDM from loops with heavy $H^\pm$ have also been found in flavor-changing Higgs decays $h \to b\bar{s}$ and $h \to s\bar{b}$, in [48]. In both works, the role of a large triple Higgs coupling $\lambda_{hH^+H^-}$ has been pointed out.

B. HEFT coefficients from nondecoupling heavy Higgs bosons

Finally, we put together here all the analytical results for the HEFT coefficients found in the previous section by solving the full set of matching equations. We provide these results in terms of the HEFT coefficients that define the BSM contributions from the 2HDM with respect to the SM. These are the following (we add explicitly here the label 2HDM for completeness):

$$\Delta a|_{2\text{HDM}} = 1 - s_{\beta-\alpha},$$

$$\Delta b|_{2\text{HDM}} = -c_{\beta-\alpha}^2(1 - 2c_{\beta-\alpha}^2 + 2c_{\beta-\alpha}s_{\beta-\alpha}\cot 2\beta),$$

$$\Delta\kappa_3|_{2\text{HDM}} = 1 - s_{\beta-\alpha}(1 + 2c_{\beta-\alpha}^2) - c_{\beta-\alpha}^2\left(-2s_{\beta-\alpha}\frac{m_{12}^2}{m_h^2 s_\beta c_\beta} + 2c_{\beta-\alpha}\cot 2\beta\left(1 - \frac{m_{12}^2}{m_h^2 s_\beta c_\beta}\right)\right),$$

$$\begin{aligned}\Delta\kappa_4|_{2\text{HDM}} = -\frac{c_{\beta-\alpha}^2}{3}\Bigg(&-7 + 64c_{\beta-\alpha}^2 - 76c_{\beta-\alpha}^4 + 12(1 - 6c_{\beta-\alpha}^2 + 6c_{\beta-\alpha}^4)\frac{m_{12}^2}{m_h^2 s_\beta c_\beta}\\ &+ 4c_{\beta-\alpha}s_{\beta-\alpha}\cot 2\beta\left(-13 + 38c_{\beta-\alpha}^2 - 3(-5 + 12c_{\beta-\alpha}^2)\frac{m_{12}^2}{m_h^2 s_\beta c_\beta}\right)\\ &+ 4c_{\beta-\alpha}^2\cot^2 2\beta\left(3c_{\beta-\alpha}^2 - 16s_{\beta-\alpha}^2 + 3(-1 + 6s_{\beta-\alpha}^2)\frac{m_{12}^2}{m_h^2 s_\beta c_\beta}\right)\Bigg),\end{aligned}$$

$$a_{h\gamma\gamma}|_{2\text{HDM}} = -\frac{s_{\beta-\alpha}}{48\pi^2},$$

$$a_{h\gamma Z}|_{2\text{HDM}} = -\frac{(2c_w^2 - 1)s_{\beta-\alpha}}{96c_w^2\pi^2}. \tag{5.12}$$

Some comments are in order. First, for shortness, in the previous formulas we have used again a compact form. To get the explicit result in terms of the 2HDM input parameters, the values of $s_{\beta-\alpha}$, s_β, c_β, and $\cot 2\beta$ given in Eq. (3.12) should be plugged into all these formulas. Then, the first conclusion is that these HEFT coefficients, capturing the nondecoupling effects from the heavy Higgs bosons in the 2HDM, depend on the subset of input parameters given by $c_{\beta-\alpha}$, $\tan\beta$, m_h, and m_{12}. Second, the above results are valid for arbitrary $-1 \leq c_{\beta-\alpha} \leq 1$; therefore, they set the coefficient values for the generic scenario with misalignment ($c_{\beta-\alpha} \neq 0$). Third, in the case of an scenario with alignment, i.e., with $c_{\beta-\alpha} = 0$, we get vanishing LO HEFT Δ's. More interestingly, we get nonvanishing values in this alignment limit for the NLO HEFT coefficients $a_{h\gamma\gamma}$ and $a_{h\gamma Z}$. Specifically, we get

$$\Delta a|_{2\text{HDM}}^{\text{al}} = 0,$$

$$\Delta b|_{2\text{HDM}}^{\text{al}} = 0,$$

$$\Delta\kappa_3|_{2\text{HDM}}^{\text{al}} = 0,$$

$$\Delta\kappa_4|_{2\text{HDM}}^{\text{al}} = 0,$$

$$a_{h\gamma\gamma}|_{2\text{HDM}}^{\text{al}} = -\frac{1}{48\pi^2},$$

$$a_{h\gamma Z}|_{2\text{HDM}}^{\text{al}} = -\frac{2c_w^2 - 1}{96c_w^2\pi^2}. \tag{5.13}$$

Fourth, in the case of an scenario with quasialignment, namely, with small but not vanishing $|c_{\beta-\alpha}| \ll 1$, we can approximate the above results in Eq. (5.12) by doing an additional Taylor expansion in powers of the small parameter $c_{\beta-\alpha}$ and keeping just the leading term in this expansion, which for the LO HEFT Δ's is of $\mathcal{O}(c_{\beta-\alpha}^2)$.

Thus, we get the following results for these Δ's in this quasialignment (qal) scenario:

$$\Delta a|_{2\text{HDM}}^{\text{qal}} = \frac{c_{\beta-\alpha}^2}{2},$$

$$\Delta b|_{2\text{HDM}}^{\text{qal}} = -c_{\beta-\alpha}^2,$$

$$\Delta\kappa_3|_{2\text{HDM}}^{\text{qal}} = -c_{\beta-\alpha}^2\left(\frac{3}{2} - 2\frac{m_{12}^2}{m_h^2}\frac{1 + t_\beta^2}{t_\beta}\right),$$

$$\Delta\kappa_4|_{2\text{HDM}}^{\text{qal}} = c_{\beta-\alpha}^2\left(\frac{7}{3} - 4\frac{m_{12}^2}{m_h^2}\frac{1 + t_\beta^2}{t_\beta}\right). \tag{5.14}$$

Fifth, we remark that in the previous quasialignment limit we find some simple correlations among the LO HEFT coefficients that we find interesting to comment:

$$\Delta a|_{2\text{HDM}}^{\text{qal}} = -\frac{1}{2}\Delta b|_{2\text{HDM}}^{\text{qal}}, \tag{5.15}$$

$$\Delta\kappa_3|_{2\text{HDM}}^{\text{qal}} = -\frac{9}{14}\Delta\kappa_4|_{2\text{HDM}}^{\text{qal}} - \frac{4}{7}c_{\beta-\alpha}^2\frac{m_{12}^2}{m_h^2}\frac{1 + t_\beta^2}{t_\beta}. \tag{5.16}$$

The first one is independent on m_{12} and $\tan\beta$. Notice the different correlation between these two Δ's here in the 2HDM and in the SMEFT which was commented at the end of Sec. II. For the result regarding the κ's in Eq. (5.16), the correlation gets further simplified if $m_{12} = 0$:

$$\Delta\kappa_3|_{2\text{HDM}}^{\text{qal}} = -\frac{9}{14}\Delta\kappa_4|_{2\text{HDM}}^{\text{qal}} \qquad (m_{12} = 0). \tag{5.17}$$

On the other hand, one can also write together $\Delta\kappa_3|_{2\text{HDM}}^{\text{qal}}$ and $\Delta\kappa_4|_{2\text{HDM}}^{\text{qal}}$ in Eq. (5.14) in the following alternative form:

$$2\Delta\kappa_3|^{\text{qal}}_{\text{2HDM}} + \Delta\kappa_4|^{\text{qal}}_{\text{2HDM}} = -\frac{2}{3}c^2_{\beta-\alpha}, \qquad (5.18)$$

which is interesting because it is independent on the value of m_{12} and $\tan\beta$. Then, from Eqs. (5.14) and (5.18), it is immediate to check that the following relation among the four Δ's holds in the quasialignment case:

$$2\Delta\kappa_3|^{\text{qal}}_{\text{2HDM}} + \Delta\kappa_4|^{\text{qal}}_{\text{2HDM}} = \frac{2}{3}\Delta b|^{\text{qal}}_{\text{2HDM}} = -\frac{4}{3}\Delta a|^{\text{qal}}_{\text{2HDM}}.$$
$$(5.19)$$

Our final comment refers to the comparison of our results for the HEFT coefficients with those found in [21]. They do not consider one-loop generated coefficients and work close to the alignment limit; thus, we can compare only our simplified results in the quasialignment limit in Eq. (5.14) with their results. Except for Δa, where we agree, the rest of Δ's are clearly different. In fact, they express the results for the HEFT coefficients in terms of a common heavy mass Λ and the splittings among the heavy Higgs boson masses which they assume to be of $\mathcal{O}(v)$. They also assume a value for $c_{\beta-\alpha}$ of $\mathcal{O}(v^2/\Lambda^2)$. None of these assumptions are done in the present work, since we deal with generic input $c_{\beta-\alpha}$ and generic mass splittings, so these different results are not surprising. Our interpretation of these differences is that they follow different paths to move through the 2HDM parameter space in the heavy mass limit. In particular, they "freeze" the values of the triple Higgs couplings λ_x by their perturbativity requirement, whereas we do not. Thus, they do not get non-decoupling effects from the heavy Higgs bosons, whereas we do.

VI. NUMERICAL RESULTS

In this section, we present our numerical results for the HEFT coefficients in Eq. (5.12) in terms of the 2HDM input parameters. First, we comment on the one-loop generated coefficients $a_{h\gamma\gamma}|_{\text{2HDM}}$ and $a_{h\gamma Z}|_{\text{2HDM}}$. Since they depend only on the value of $s_{\beta-\alpha}$, and this lies in the interval $0 \le s_{\beta-\alpha} \le 1$, then the predicted coefficients in Eq. (5.12) fulfill

$$-\frac{1}{48\pi^2} \le a_{h\gamma\gamma}|_{\text{2HDM}} \le 0, \qquad (6.1)$$

$$-\frac{2c^2_{\text{w}}-1}{96c^2_{\text{w}}\pi^2} \le a_{h\gamma Z}|_{\text{2HDM}} \le 0. \qquad (6.2)$$

Then, they are numerically small quantities, as is expected since they are one-loop generated coefficients. In particular, the values reached for alignment are the following:

$$a_{h\gamma\gamma}|^{\text{al}}_{\text{2HDM}} = -0.00211, \qquad (6.3)$$

$$a_{h\gamma Z}|^{\text{al}}_{\text{2HDM}} = -0.000944. \qquad (6.4)$$

Next, we comment on the LO HEFT coefficients. We start with the simplest case of $m_{12} = 0$. The numerical predictions for $\Delta a|_{\text{2HDM}}$, $\Delta b|_{\text{2HDM}}$, $\Delta\kappa_3|_{\text{2HDM}}$, and $\Delta\kappa_4|_{\text{2HDM}}$ in this $m_{12} = 0$ case depend just on $c_{\beta-\alpha}$ and $\tan\beta$. Their predictions in terms of these two parameters are presented in Fig. 12, as contours lines in the $(c_{\beta-\alpha}, \tan\beta)$ plane. The predictions in the generic (full) case, using Eq. (5.12), are collected in the left plots and the predictions in the quasialignment (approximate) case, using Eq. (5.14), in the right plots. The black solid lines in these plots represent the predictions where the Δ's are zero. This always coincides with the alignment limit, but the Δ's can also vanish in other regions with concrete configurations of the 2HDM input parameters. The intervals displayed in the axes of these plots are chosen to roughly cover the allowed experimental values. In particular, the interval explored in $c_{\beta-\alpha}$ is shortened to $|c_{\beta-\alpha}| < 0.2$ and the one in $\tan\beta$ is shortened to $0.5 < \tan\beta < 20$. The numerical values predicted in those reduced intervals range roughly as follows: $0 < \Delta a|_{\text{2HDM}} < 0.02$, $-0.2 < \Delta b|_{\text{2HDM}} < 0.12$, $-0.22 < \Delta\kappa_3|_{\text{2HDM}} < 0.11$, and $-0.05 < \Delta\kappa_4|_{\text{2HDM}} < 4.5$. Their maximum values are reached for the largest considered $|c_{\beta-\alpha}|$ values and the largest considered $\tan\beta$ values (except for Δa that is independent on $\tan\beta$). Regarding the comparison between the generic and quasialignment results, we see that the predictions for $\Delta a|_{\text{2HDM}}$ (left) versus those for $\Delta a|^{\text{qal}}_{\text{2HDM}}$ (right) look very similar. We also see that the predictions for the other Δ's look also very similar in the low region of $\tan\beta$. The largest differences among generic and quasialignment occur in the upper right corner for Δb and $\Delta\kappa_3$ and in the upper left corner for $\Delta\kappa_4$. In any case, we can conclude that the simple formulas in Eq. (5.14) (applied for $m_{12} = 0$) provide a very good approximation to the full result of Eq. (5.12) in the low $\tan\beta < 2$ region.

The values of $\Delta\kappa_3$ and $\Delta\kappa_4$ for the $m_{12} \neq 0$ case are explored in Fig. 13. We consider two different input values of $m_{12} = 100$ GeV and $m_{12} = 400$ GeV. The same intervals in the axes as before are considered in these contours in the $(c_{\beta-\alpha}, \tan\beta)$ plane for the $m_{12} \neq 0$ case. Looking at the generic plots (left), we see that the size of $\Delta\kappa_3$ increases for larger m_{12} reaching values of up to 10 in the upper left corner (with $\tan\beta$ close to 20) of the second plot for $m_{12} = 400$ GeV. The size of $\Delta\kappa_4$ also reaches the largest values of about 5 for the larger $m_{12} = 400$ GeV case, but it happens at lower values of $\tan\beta$ below 10. In addition, $\Delta\kappa_4$ can also reach large, but negative, values below -20 in the regions of large $\tan\beta$ and far from the alignment limit in both cases where $m_{12} = 100, 400$ GeV. Comparing the plots on the left (generic) with those in the right (quasialignment), we find again that these latter provide a reasonable approximation in the low $\tan\beta$ region, roughly below 5 for $\Delta\kappa_3$ and below 2 for $\Delta\kappa_4$.
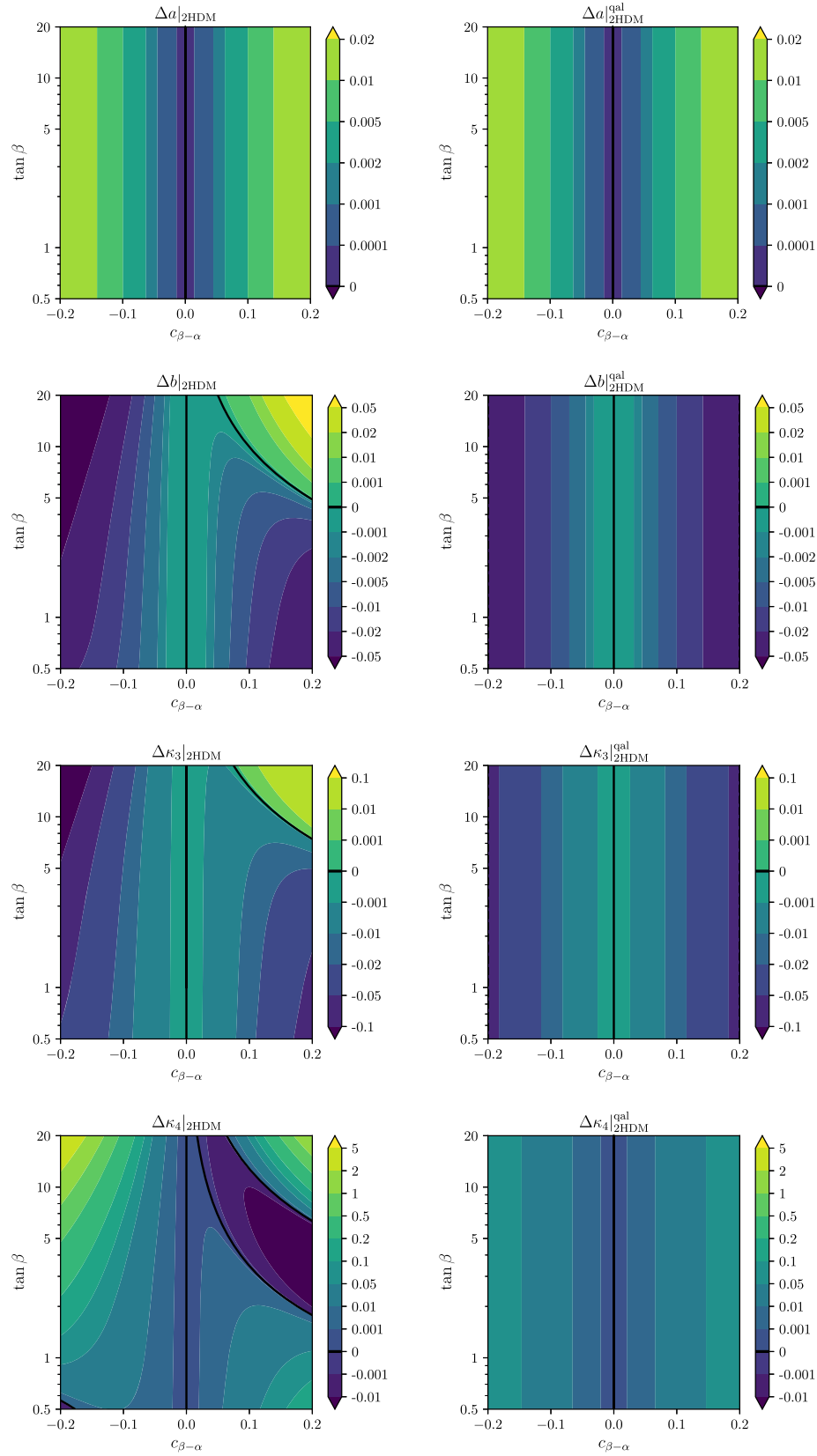
FIG. 12. LO HEFT parameters Δa, Δb, $\Delta \kappa_3$, and $\Delta \kappa_4$ from 2HDM: contours in the $(c_{\beta-\alpha}, \tan \beta)$ plane for $m_{12} = 0$. Generic (full) case in left plots, using Eq. (5.12), versus quasialignment (approximate) case in right plots, using Eq. (5.14).
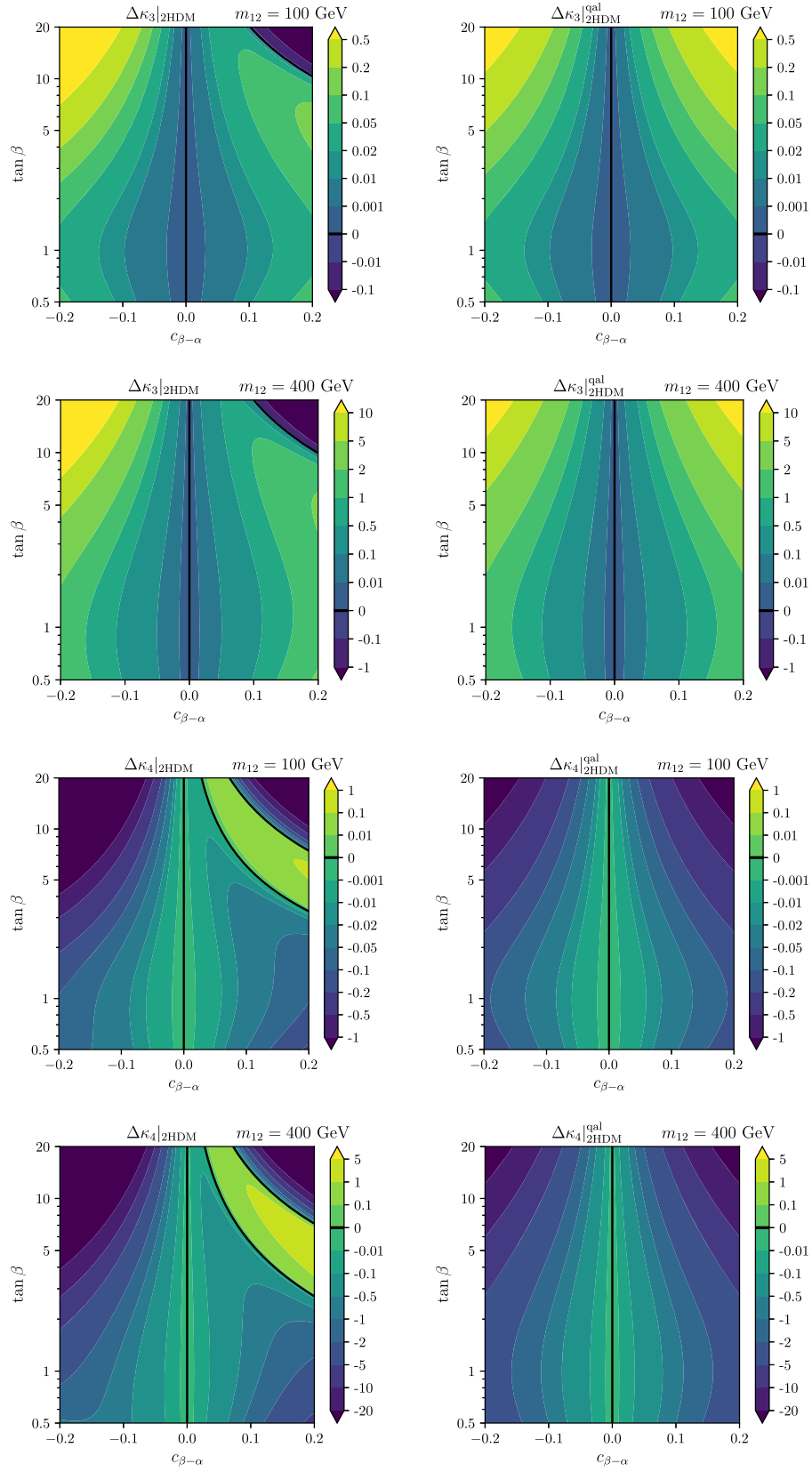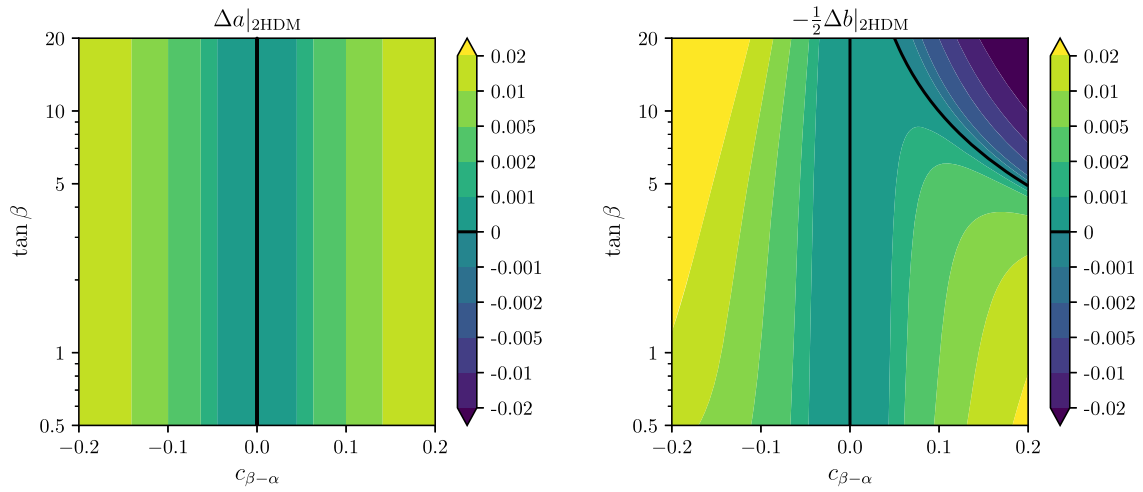
FIG. 13. LO HEFT parameters $\Delta\kappa_3$ and $\Delta\kappa_4$ from 2HDM: contours in the $(c_{\beta-\alpha}, \tan\beta)$ plane for $m_{12} \neq 0$. Generic (full) case in left plots, using Eq. (5.12), versus quasialignment (approximate) case in right plots, using Eq. (5.14).

FIG. 14. Correlations between LO HEFT coefficients from the 2HDM $\Delta a|_{2HDM}$ and $-\frac{1}{2}\Delta b|_{2HDM}$ in the generic (full) case, using Eq. (5.12).
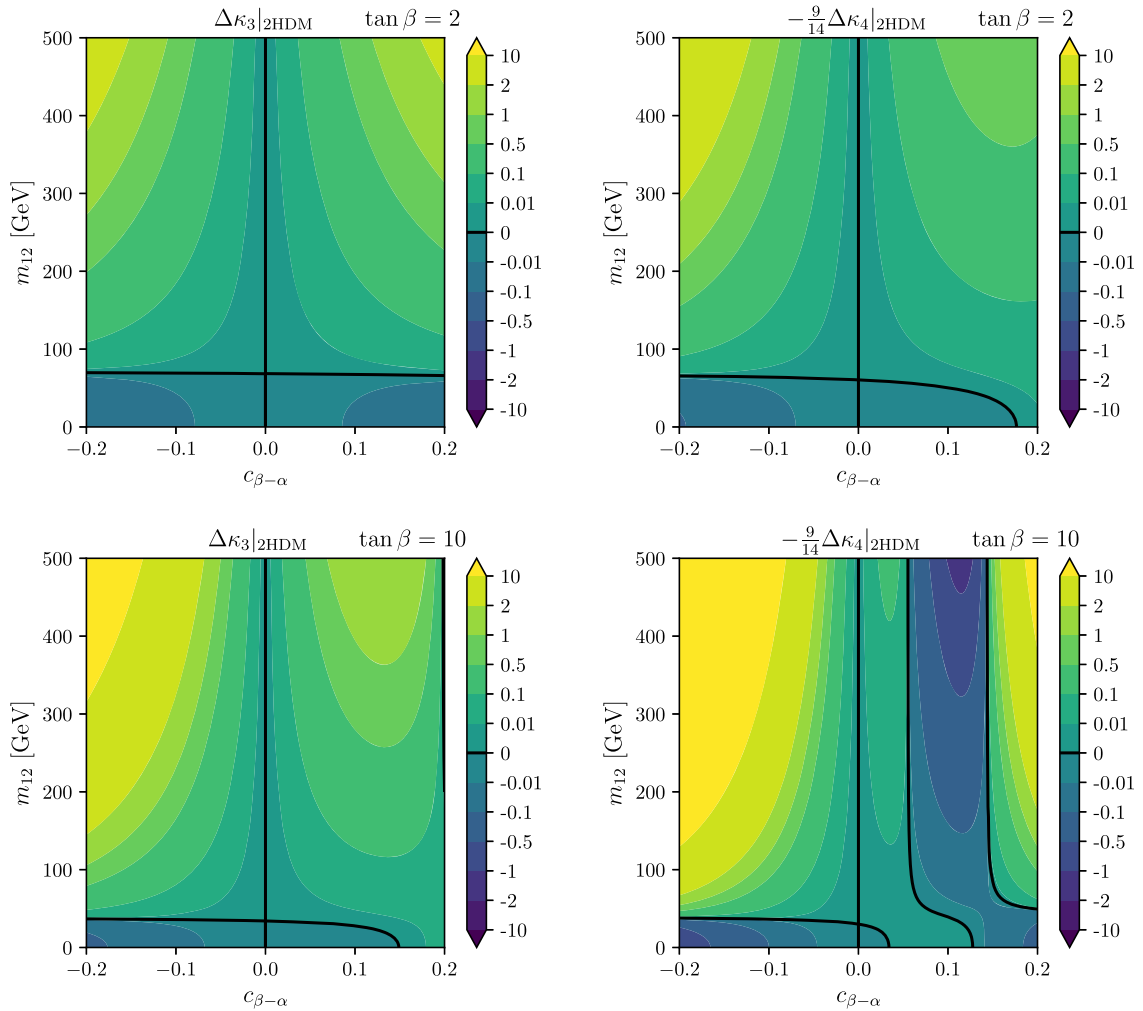
FIG. 15. Correlations between LO HEFT coefficients from the 2HDM $\Delta\kappa_3|_{2HDM}$ and $-\frac{9}{14}\Delta\kappa_4|_{2HDM}$ in the generic (full) case, using Eq. (5.12).

Finally, we study numerically the interesting correlations found among the HEFT coefficients, Δa versus Δb and $\Delta \kappa_3$ versus $\Delta \kappa_4$ in Figs. 14 and 15, respectively. Notice that we have chosen to plot in Figs. 14 and 15 the quantities $\Delta a|_{2\mathrm{HDM}}$ versus $-\frac{1}{2}\Delta b|_{2\mathrm{HDM}}$ and $\Delta \kappa_3|_{2\mathrm{HDM}}$ versus $-\frac{9}{14}\Delta \kappa_4|_{2\mathrm{HDM}}$ motivated by the particular combinations appearing in the quasialignment results of Eqs. (5.15) and (5.16), respectively. These are all studied for the general case with misalignment; namely, we use the full formulas in Eq. (5.12). One can see in Fig. 14 that a clear correlation between $\Delta a|_{2\mathrm{HDM}}$ and $-\frac{1}{2}\Delta b|_{2\mathrm{HDM}}$ is manifested for $\tan\beta < 5$, and this correlation is well represented by our approximate results of the quasialignment scenario. Regarding $\Delta \kappa_3$ and $\Delta \kappa_4$, we see in the upper plots in Fig. 15 that for low $\tan\beta = 2$ a clear correlation between $\Delta \kappa_3|_{2\mathrm{HDM}}$ and $-\frac{9}{14}\Delta \kappa_4|_{2\mathrm{HDM}}$ is manifested for $m_{12} < 300$ GeV. Increasing $\tan\beta$ worsens this correlation. From the two lower plots, for $\tan\beta = 10$, we see that this correlation manifests only in the very narrow region with very small $c_{\beta-\alpha}$ values close to alignment. Therefore, this correlation is well represented by our approximated formulas of the quasialignment scenario for sufficiently small $c_{\beta-\alpha}$ values, namely, for $|c_{\beta-\alpha}| < 0.05$.

VII. CONCLUSIONS

In this work, we have computed the most relevant nondecoupling effects from the BSM Higgs bosons within the 2HDM, H, A, and $H^{\pm}$. The light Higgs boson h is assumed here to be the one observed experimentally with a mass $m_h \sim 125$ GeV. Our simple hypothesis for the masses of the BSM Higgs bosons is that they are very heavy compared to the EW masses m_Z, m_W, m_f, m_h, v, and m_{12}. We have worked within the framework of EFTs, and, more concretely, we have assumed the HEFT to be the proper EFT to describe the low-energy effects from the 2HDM heavy Higgs bosons. We focus here on just the bosonic sector. Specifically, we have found that the low-energy effects that result from the integration of the heavy Higgs boson modes H, A, and $H^{\pm}$ can be collected into a set of HEFT coefficients which turn out not to be suppressed by inverse powers of the heavy masses but instead are constant with these masses. Those values constant with m_{heavy} summarize the nondecoupling effects from the heavy Higgs bosons.

Our approach to compute such nondecoupling effects is by solving the matching between the 2HDM and the HEFT at low energies compared to the heavy masses. Instead of the usual matching at the Lagrangian level, we impose here a more physical matching which requires the equality between the amplitudes predicted by the 2HDM in the heavy mass limit of the BSM Higgs bosons with those predicted by the HEFT. Furthermore, we do this matching at the amplitude level by considering specific processes involving the light Higgs boson in the external legs that include scattering and decays. Concretely, we have studied and solved the matching between the 2HDM and the HEFT amplitudes for the following seven processes: $h \to WW^* \to Wf\bar{f}'$, $h \to ZZ^* \to Zf\bar{f}$, $W^+W^- \to hh$, $ZZ \to hh$, $hh \to hh$, $h \to \gamma\gamma$, and $h \to \gamma Z$. All amplitudes have been computed in a covariant R_ξ gauge to get control on the gauge invariance of the results. The amplitudes for the five first processes have been computed at the tree level in the HEFT, 2HDM, and also the SM for comparison. The amplitudes of the two last decays have been computed to one-loop level in the three models. We have shown that the expansion of the 2HDM amplitudes in inverse powers of the heavy masses provides convergent results for the HEFT coefficients in the heavy mass limit. In addition, we have identified the triple couplings of the light Higgs with the heavy Higgs bosons as being the responsible for the nondecoupling effects from the heavy Higgs bosons in the amplitudes.

The nondecoupling effects found here are summarized in the values of the HEFT coefficients collected in Eq. (5.12) which have been given in terms of the input 2HDM parameters. These input parameters have been chosen in this work to be m_h, m_H, m_A, $m_{H^\pm}$, v, $c_{\beta-\alpha}$, $\tan\beta$, and m_{12}. In fact, the analytical results found here for the HEFT coefficients turn out to depend on just a subset of them. Concretely, Δa, $a_{h\gamma\gamma}$, and $a_{h\gamma Z}$ are given in terms of just $c_{\beta-\alpha}$. Δb is given in terms of $c_{\beta-\alpha}$ and $\tan\beta$, and $\Delta \kappa_3$ and $\Delta \kappa_4$ are given on terms of $c_{\beta-\alpha}$, $\tan\beta$, and m_{12}. We wish to emphasize that these results are valid for a generic value of $c_{\beta-\alpha}$; i.e., they apply for the generic misalignment case. We have also provided their analytical values in the simpler cases of alignment with $c_{\beta-\alpha} = 0$ and of quasialignment with $c_{\beta-\alpha} \ll 1$, summarized in Eqs. (5.13) and (5.14), respectively. In looking at those solutions from the matching, we have detected some correlations among the HEFT coefficients, which can be of much interest in the future colliders searches of BSM physics.

Finally, we have also explored numerically the values of the HEFT coefficients as a function of the 2HDM input parameters. For the considered intervals in the relevant 2HDM input parameters, which are roughly allowed by the present constraints, we find values of $0 < \Delta a|_{2\mathrm{HDM}} < 0.02$, $-0.2 < \Delta b|_{2\mathrm{HDM}} < 0.12$, $-0.22 < \Delta \kappa_3|_{2\mathrm{HDM}} < 0.11$, and $-0.05 < \Delta \kappa_4|_{2\mathrm{HDM}} < 4.5$ in the simplest case of $m_{12} = 0$.

The correlations among the HEFT coefficients have also been explored numerically. We have found that a clear correlation between $\Delta a|_{2\mathrm{HDM}}$ and $-\frac{1}{2}\Delta b|_{2\mathrm{HDM}}$ is manifested for $\tan\beta < 5$, and this correlation is well represented by our approximate results of the quasialignment scenario. Regarding the κ's, we have found that for low $\tan\beta = 2$ a clear correlation between $\Delta \kappa_3|_{2\mathrm{HDM}}$ and $-\frac{9}{14}\Delta \kappa_4|_{2\mathrm{HDM}}$ is manifested for $m_{12} < 300$ GeV. Increasing $\tan\beta$ worsens this correlation. For instance, for $\tan\beta = 10$, we see that this correlation manifests only in the very narrow region

with very small $c_{\beta-\alpha}$ values close to alignment. Therefore, this correlation is well represented by our approximated formulas of the quasialignment scenario for sufficiently small $c_{\beta-\alpha}$ values, namely, for $|c_{\beta-\alpha}| < 0.05$.

All in all, we conclude that the nondecoupling effects found in this work could serve in the future as a guide to look for indirect hints from the 2HDM heavy Higgs bosons, even if they are too heavy to be produced directly at colliders.

APPENDIX A: RELEVANT FEYNMAN RULES

In this section, we provide in Table I all relevant Feynman rules for the computation of the scattering and decay amplitudes discussed in this work. We include only those interactions among fields that are external legs in the considered processes. The three models in consideration, SM, HEFT, and 2HDM, are showed for comparison. The relevant Feynman rules for Higgs boson scalar

TABLE I. Relevant Feynman rules involving the SM-like Higgs boson in the SM, HEFT, and 2HDM for comparison. All momenta are incoming. The relations among the tree-level EW parameters are as in the SM: $m_W = (gv)/2$, $m_Z = m_W/c_{\rm w}$, and $m_h^2 = 2\lambda v^2$.
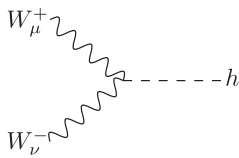
Interaction	SM	HEFT	2HDM
W_μ^+ ⋯ h / W_ν^-	$\frac{2im_W^2}{v} g^{\mu\nu}$	$\frac{2im_W^2}{v} a g^{\mu\nu}$	$\frac{2im_W^2}{v} s_{\beta-\alpha} g^{\mu\nu}$
Z_μ ⋯ h / Z_ν	$\frac{2im_Z^2}{v} g^{\mu\nu}$	$\frac{2im_Z^2}{v} a g^{\mu\nu}$	$\frac{2im_Z^2}{v} s_{\beta-\alpha} g^{\mu\nu}$
$\gamma_\mu(k_1)$ ⋯ h / $\gamma_\nu(k_2)$	0	$\frac{2g^2 s_{\rm w}^2}{v} a_{h\gamma\gamma}(k_1 \cdot k_2 g^{\mu\nu} - k_2^\mu k_1^\nu)$	0
$\gamma_\mu(k_1)$ ⋯ h / $Z_\nu(k_2)$	0	$\frac{2g^2 s_{\rm w} c_{\rm w}}{v} a_{h\gamma Z}(k_1 \cdot k_2 g^{\mu\nu} - k_2^\mu k_1^\nu)$	0
W_μ^+ ⋯ h, h / W_ν^-	$i\frac{g^2}{2} g^{\mu\nu}$	$i\frac{g^2}{2} b g^{\mu\nu}$	$i\frac{g^2}{2} g^{\mu\nu}$
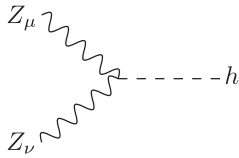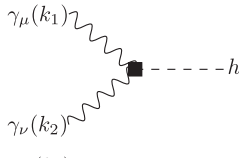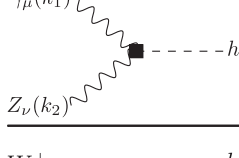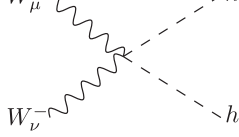
(Table continued)

TABLE I. *(Continued)*

Interaction	SM	HEFT	2HDM
	$i\frac{g^2}{2c_w^2}g^{\mu\nu}$	$i\frac{g^2}{2c_w^2}bg^{\mu\nu}$	$i\frac{g^2}{2c_w^2}g^{\mu\nu}$
	$-6i\lambda v$	$-6i\lambda v\kappa_3$	$-6i\lambda_{hhh}v$
	$-6i\lambda$	$-6i\lambda\kappa_4$	$-6i\lambda_{hhhh}$

interactions in the 2HDM can also be found in Eqs. (3.4)–(3.7).

APPENDIX B: ONE-LOOP FUNCTIONS

The one-loop computation is performed with dimensional regularization in $D = 4 - \epsilon$ dimensions, and we use the standard definitions for the associated divergence:

$$\Delta_\epsilon = \frac{1}{4-D} - \gamma_E + \log(4\pi), \tag{B1}$$

where μ_0 is the usual scale. We implement the compact notation for the momentum integral given by

$$\int_k = \mu_0^{4-D} \int \frac{d^D k}{(2\pi)^D}. \tag{B2}$$

To display some results, we also use the scalar two- and three-point one-loop integral functions in the Passarino-Veltman notation [49], with the following conventions:

$$\frac{i}{16\pi^2} A_0(m_1) = \int_k \frac{1}{[k^2 - m_1^2]},$$
$$\frac{i}{16\pi^2} B_0(q_1, m_1, m_2) = \int_k \frac{1}{[k^2 - m_1^2][(k+q_1)^2 - m_2^2]},$$
$$\frac{i}{16\pi^2} C_0(q_1, q_2, m_1, m_2, m_3) = \int_k \frac{1}{[k^2 - m_1^2][(k+q_1)^2 - m_2^2][(k+q_1+q_2)^2 - m_3^2]}. \tag{B3}$$

We introduce

$$f(r) = -\frac{1}{4}\log^2\left(-\frac{1-\sqrt{1-r}}{1+\sqrt{1-r}}\right) = \begin{cases} \arcsin^2\left(\frac{1}{\sqrt{r}}\right) & r \geq 1, \\ -\frac{1}{4}\left(\ln\left(\frac{1+\sqrt{1-r}}{1-\sqrt{1-r}}\right) - i\pi\right)^2 & 0 < r < 1 \end{cases} \tag{B4}$$

and

$$g(r) = -\frac{1}{2}\sqrt{1-r}\log\left(-\frac{1-\sqrt{1-r}}{1+\sqrt{1-r}}\right) = \begin{cases} \sqrt{r-1}\arcsin\left(\frac{1}{\sqrt{r}}\right) & r \geq 1, \\ \frac{1}{2}\sqrt{1-r}\left(\ln\left(\frac{1+\sqrt{1-r}}{1-\sqrt{1-r}}\right) - i\pi\right) & 0 < r < 1, \end{cases} \tag{B5}$$

with the relations

$$B_0(q, M, M) = \Delta_\epsilon + \log\left(\frac{\mu_0^2}{M^2}\right) + 2 - 2g\left(\frac{4M^2}{q^2}\right),$$

$$C_0(0, q, M, M, M) = -\frac{2}{q^2}f\left(\frac{4M^2}{q^2}\right). \tag{B6}$$

The relevant regime for the matching in Eq. (5.10) is large r, in which case

$$f(r)|_{r\gg1} \sim \frac{1}{r} + \frac{1}{3r^2} + \mathcal{O}(r^{-3}),$$

$$g(r)|_{r\gg1} \sim 1 - \frac{1}{3r} - \frac{2}{15r^2} + \mathcal{O}(r^{-3}). \tag{B7}$$

[1] G. Aad *et al.* (ATLAS Collaboration), Phys. Lett. B **716**, 1 (2012).

[2] S. Chatrchyan *et al.* (CMS Collaboration), Phys. Lett. B **716**, 30 (2012).

[3] G. Aad *et al.* (ATLAS, CMS Collaborations), Phys. Rev. Lett. **114**, 191803 (2015).

[4] I. Brivio and M. Trott, Phys. Rep. **793**, 1 (2019).

[5] A. Dobado and D. Espriu, Prog. Part. Nucl. Phys. **115**, 103813 (2020).

[6] J. F. Gunion, H. E. Haber, G. L. Kane, and S. Dawson, *The Higgs Hunter's Guide* (Brookhaven National Laboratory, Upton, 2000), Vol. 80.

[7] G. C. Branco, P. M. Ferreira, L. Lavoura, M. N. Rebelo, M. Sher, and J. P. Silva, Phys. Rep. **516**, 1 (2012).

[8] T. Appelquist and J. Carazzone, Phys. Rev. D **11**, 2856 (1975).

[9] M. J. Herrero and E. Ruiz Morales, Nucl. Phys. **B418**, 431 (1994).

[10] M. J. Herrero and E. Ruiz Morales, Nucl. Phys. **B437**, 319 (1995).

[11] H. Bélusca-Maïto, A. Falkowski, D. Fontes, J. C. Romão, and J. a. P. Silva, Eur. Phys. J. C **77**, 176 (2017).

[12] S. Dawson, D. Fontes, S. Homiller, and M. Sullivan, Phys. Rev. D **106**, 055012 (2022).

[13] U. Banerjee, J. Chakrabortty, C. Englert, S. U. Rahaman, and M. Spannowsky, Phys. Rev. D **107**, 055007 (2023).

[14] U. Banerjee, J. Chakrabortty, C. Englert, W. Naskar, S. U. Rahaman, and M. Spannowsky, arXiv:2303.05224.

[15] R. Alonso, E. E. Jenkins, and A. V. Manohar, Phys. Lett. B **754**, 335 (2016).

[16] R. Alonso, E. E. Jenkins, and A. V. Manohar, J. High Energy Phys. 08 (2016) 101.

[17] A. Falkowski and R. Rattazzi, J. High Energy Phys. 10 (2019) 255.

[18] T. Cohen, N. Craig, X. Lu, and D. Sutherland, J. High Energy Phys. 03 (2021) 237.

[19] T. Cohen, N. Craig, X. Lu, and D. Sutherland, J. High Energy Phys. 12 (2021) 003.

[20] S. Kanemura and R. Nagai, J. High Energy Phys. 03 (2022) 194.

[21] S. Dawson, D. Fontes, C. Quezada-Calonge, and J. J. Sanz-Cillero, arXiv:2305.07689.

[22] M. Herrero and R. A. Morales, Phys. Rev. D **102**, 075040 (2020).

[23] M. J. Herrero and R. A. Morales, Phys. Rev. D **104**, 075013 (2021).

[24] M. J. Herrero and R. A. Morales, Phys. Rev. D **106**, 073008 (2022).

[25] R. L. Delgado, A. Dobado, and F. J. Llanes-Estrada, J. High Energy Phys. 02 (2014) 121.

[26] R. L. Delgado, A. Dobado, and F. J. Llanes-Estrada, Phys. Rev. Lett. **114**, 221803 (2015).

[27] I. n. Asiáin, D. Espriu, and F. Mescia, Phys. Rev. D **105**, 015009 (2022).

[28] I. n. Asiáin, D. Espriu, and F. Mescia, Phys. Rev. D **107**, 115005 (2023).

[29] Anisha, O. Atkinson, A. Bhardwaj, C. Englert, and P. Stylianou, J. High Energy Phys. 10 (2022) 172.

[30] E. E. Jenkins, A. V. Manohar, and M. Trott, J. High Energy Phys. 10 (2013) 087.

[31] E. E. Jenkins, A. V. Manohar, and M. Trott, J. High Energy Phys. 01 (2014) 035.

[32] R. Alonso, E. E. Jenkins, A. V. Manohar, and M. Trott, J. High Energy Phys. 04 (2014) 159.

[33] A. Dedes, W. Materkowska, M. Paraskevas, J. Rosiek, and K. Suxho, J. High Energy Phys. 06 (2017) 143.

[34] M. Misiak, M. Paraskevas, J. Rosiek, K. Suxho, and B. Zglinicki, J. High Energy Phys. 02 (2019) 051.

[35] I. Brivio, S. Bruggisser, E. Geoffray, W. Killian, M. Krämer, M. Luchmann, T. Plehn, and B. Summ, SciPost Phys. **12**, 036 (2022).

[36] D. Domenech, M. J. Herrero, R. A. Morales, and M. Ramos, Phys. Rev. D **106**, 115027 (2022).

[37] K. Fujikawa, B. Lee, and A. Sanda, Phys. Rev. D **6**, 2923 (1972).

[38] L. Faddeev and V. Popov, Phys. Lett. **25B**, 29 (1967).

[39] M. Aoki, S. Kanemura, K. Tsumura, and K. Yagyu, Phys. Rev. D **80**, 015017 (2009).

[40] S. L. Glashow and S. Weinberg, Phys. Rev. D **15**, 1958 (1977).

[41] F. Arco, S. Heinemeyer, and M. J. Herrero, Eur. Phys. J. C **80**, 884 (2020).

[42] F. Arco, S. Heinemeyer, and M. J. Herrero, Eur. Phys. J. C **82**, 536 (2022).

[43] T. Hahn, Comput. Phys. Commun. **140**, 418 (2001).

[44] T. Hahn and M. Perez-Victoria, Comput. Phys. Commun. **118**, 153 (1999).

[45] W. J. Marciano, C. Zhang, and S. Willenbrock, Phys. Rev. D **85**, 013002 (2012).

[46] D. Fontes, J. C. Romão, and J. a. P. Silva, J. High Energy Phys. 12 (2014) 043.

[47] F. Arco, S. Heinemeyer, and M. J. Herrero, Phys. Lett. B **835**, 137548 (2022).

[48] F. Arco, S. Heinemeyer, and M. J. Herrero, arXiv:2306.07958.

[49] G. Passarino and M. Veltman, Nucl. Phys. **B160**, 151 (1979).